Hindawi
International Transactions on Electrical Energy Systems
Volume 2022, Article ID 1281248, 23 pages
https://doi.org/10.1155/2022/1281248

Research Article

LSTM Recurrent Neural Network-Based Frequency Control Enhancement of the Power System with Electric Vehicles and Demand Management

G. Sundararajan [1] **and P. Sivakumar** [2]

[1]*Department of EEE, J. J. College of Engineering and Technology, Tiruchirappalli, Tamil Nadu, India*
[2]*Department of EEE, Rajalakshmi Engineering College, Chennai, Tamil Nadu, India*

Correspondence should be addressed to P. Sivakumar; lpssivakumar@gmail.com

Received 1 July 2022; Revised 3 September 2022; Accepted 3 October 2022; Published 31 October 2022

Academic Editor: Baseem Khan

Due to the unpredictable and stochastic nature of renewables, current power networks confront operational issues as renewable energy sources are more widely used. Frequency stability of modern power systems has been considerably harmed by fast and unpredictable power variations generated by intermittent power generation sources and flexible loads. The main objective of the power system frequency control is to ensure the generation demand balance at all times. In reality, obtaining precise estimates of the imbalance of power in both transmission and distribution systems is challenging, especially when renewable energy penetration is high. Electric vehicles have become a viable tool to reduce the occasional impact of renewable energy sources engaged in frequency regulation mainly because of vehicle-to-grid technologies and the quick output power management of EV batteries. The rapid response of EVs enhances the effectiveness of the LFC system significantly. This research work investigates a deep learning strategy based on a long short-term memory recurrent neural network to identify active power fluctuations in real-time. The new approach assesses power fluctuations from a real-time observed frequency signal precisely and quickly. The observed power fluctuations can be used as a control reference, allowing automatic generation control to maintain better system frequency and ensure optimum generation cost with the use of demand management techniques. To validate the suggested method and compare it with several classical methods, a realistic model of the Indian power system integrated with distributed generation technology is used. The simulation results clearly indicate the importance of power fluctuation identification as well as the benefits of the proposed strategy. The results clearly show a considerable improvement in response performance indices, as the maximum peak overshoot was decreased by 21.25% to 51.2%, and settling time was lowered by about 23.34% to 65.40% for the suggested control technique compared to other controllers.

1. Introduction

For many decades, load frequency control (LFC) in electrical power systems was extensively used to ensure a balance between load consumption and power production in each control area, thereby eliminating system frequency variations. Due to increased renewable energy penetration, deployment of innovative solutions such as smart grid, and modernization of the electric power system with insecure communication technologies, electric power systems increased their complexity which in turn directly affected the electric power system's operation, stability, and safety [1, 2]. The inclusion of electric vehicles (EVs) into LFC systems through an aggregator has received a lot of interest in recent years [3–8]. EVs have become a viable tool to reduce the occasional impact of renewable energy sources engaged in frequency regulation because of vehicle-to-grid technologies and the quick output power management of EV batteries. The rapid response of EVs enhances the effectiveness of the LFC system significantly. Although EVs can be used as generators or loads, unwanted frequency changes can be reduced and thus the frequency response can be improved.

To practically manage the involvement of EVs in the frequency control market, an aggregator is used. The aggregator's role is to gather and manage a group of EVs to meet frequency regulation criteria [9, 10].

Hundreds of thousands of EVs can also be connected to the grid as a massive battery energy storage system (BESS). This is possible as EVs plug into the grid when parked at a station or at home. Due to the short response time of EV batteries, a fleet of EVs working as a massive BESS is specifically successful in regulating load demand and wind power oscillations [11]. EVs aggregation into the interconnected power system can engage in both primary and secondary frequency control to help conventional power plants promptly decrease system frequency fluctuations caused by load disruptions and unpredictable renewable energy sources. In terms of primary frequency control (PFC), EVs' PFC can emulate the behavior of a turbine governor by adopting a droop control [12–19]. The author [12] presented a basic control strategy for EVs with a load estimator, in which all EVs are abruptly unplugged from the grids due to increased demand in the system. When the power of the disconnected EVs is greater than the system's power imbalance, this control strategy, however, can have negative effects on system frequency.

In secondary frequency control (SFC), an aggregation of EVs serves as a generating power source to assist an existing power generation system meet the LFC need quickly [20, 21]. EVs use bidirectional power electronic devices to communicate with the power grid, allowing them to respond to new load set-points faster than traditional generators [22]. For LFC analysis, EV-based battery storage was proposed in [20]. The usefulness of SFC with EVs in lowering the area control errors (ACEs) in a Western Danish power system is demonstrated in this simulation. Furthermore, the authors studied LFC power system topologies with EV integration in [23, 24]. LFC methods effectively control frequency fluctuation by using the SFC signal to manage EV power output.

Moreover, EV aggregators send information to the controller about EVs energy capabilities, electrical power availability, and charging status. As a result, the aggregators restructure control instructions regarding the engagement of EVs for automatic generation control to control their output power [22, 25–28].

Under unexpected and worsening changes in load conditions, it is not possible to keep the system frequency within a prescribed limit. Then, the demand management technique can be implemented using a nature-inspired algorithm to optimise system operation cost to find the flexible demand of EVs engaged by the system to maintain the supply-demand balance, which in turn is reflected in the frequency control.

Over the last few decades, algorithms inspired by the natural behavior of species that rely on beneficial properties of biological systems have evolved rapidly. Swarm intelligence systems imitate the social behavior of birds, bees, and ants. Their prominence stems from their capacity to successfully tackle real-world global optimization problems [29]. Different swarm intelligence algorithms such as Ant Colony Optimization (ACO) [30], Ant Lion Optimizer (ALO) [31], Particle Swarm Optimization (PSO) [32], Firefly Algorithm (FA) [33], and Chimp Optimization (CO) [34] are based on simple notions related to physical phenomena and evolutionary psychology. These algorithms have drawn a lot of interest since they are derivative-free, robust, and can be used to solve a variety of optimization problems. These algorithms employ the randomization idea, which shifts the efficiency of local search to global search.

However, due to their sluggish convergence speed, such single approaches are ineffective in solving optimization problems as these approaches take a long time to compute and are usually confined to the local search space. As a result, numerous optimization techniques have been merged to calculate better outputs to improve the benefits of such optimization algorithms. The efficiency of these optimization techniques, which combine the best aspects of two or three methods, has been demonstrated in terms of computing time and convergence rate. These algorithms are capable of finding optimal results more quickly than traditional algorithms. The suggested Firefly Algorithm hybridized with Flower Pollination Algorithm (FA/FPA) effectively utilizes two specific terms from the Firefly Algorithm (FA) and Flower Pollination Algorithm (FPA): exploration and exploitation. The proposed hybrid will be compared with the Firefly Algorithm (FA) and Flower Pollination Algorithm (FPA) based on their performance.

To enhance the performance of the controller, the author [35] suggested a novel resilient LFC design for multiarea power systems based on the second-order sliding mode control and an extended disturbance observer. For a hybrid isolated microgrid, the author [36] devised a new frequency control mechanism based on a disturbance observer and double sliding mode controllers. Numerous methods such as distributed control, robust control, and model predictive control were proposed to enhance the LFC's performance, though their efficiency and response time were largely dependent on the estimated imbalance of power [37–39].

Deep learning has shown promise in solving complicated nonlinear engineering issues in current history. To handle short-term load forecasting problems in individual residential families, Kong [40] suggested a prediction framework based on the long short-term memory (LSTM) recurrent neural network (RNN). The short-term load demand prediction was performed using a radial basis function neural network (RBFNN) [41]. Most existing research on power fluctuations estimate of LFC relies on disturbance observers [35, 36, 42, 43].

(i) To the best of the authors' knowledge, online power fluctuation detection using a data-driven strategy has not been resorted to in solving frequency deviation problems accompanying the application of demand management techniques.

Because of the greater penetration of renewable power generation and controllable demands in power system, rapid

and unpredictable power surges can dramatically degrade the power system's frequency performance. The goal of this research is to apply a recurrent neural network to accurately assess real-time power fluctuations from frequency measurements along with the application of demand management techniques. This paper's key contribution and novelty can be summarised as follows:

(i) An LSTM RNN is intended to provide an accurate control signal to the LFC to control the frequency of the power system.

(ii) The online application of the well-trained LSTM is used to recognize real-time power fluctuations from the recorded frequency. Control devices, such as synchronous generators and energy storage integrated EV systems, can keep the frequency in a steady condition by using identified power fluctuations.

(iii) Under unexpected and worsening changes in load conditions, it is not possible to keep system frequency within a prescribed limit. Thus, the demand management technique can be implemented using FA/FPA algorithm to optimise system operation cost to find the flexible demand of EVs engaged in the system to maintain the supply-demand balance, which is reflected in the frequency control.

(iv) With actual data on power and frequency changes, a model of the Indian power system that includes combined heat and power generation, solar photovoltaic generation, wind energy generation, and loads (including electric vehicles) is developed. The proposed algorithm is tested on this platform and compared to several conventional algorithms.

The remainder of this work is structured as follows: Section 2 describes the transfer function model of the multiarea system. Section 3 proposes the LSTM RNN method that is applied to optimise the fitness function. Section 4 narrates the FA/FPA algorithm and its application to find the optimal flexible load demand. Section 5 verifies the proposed logic using simulation results. Finally, Section 6 concludes the considered work.

2. System Model

Building an appropriate hybrid power system model for the LFC analysis is quite important. In the proposed approach, the four-area model included a renewable energy source such as a wind turbine and a photovoltaic module in addition to an electric vehicle. Controlling output power from intermittent power generation systems is difficult due to uneven variations. It is also completely different compared to nonintermittent power generation systems. There have always been difficulties with stability when power demand was greater than power generation.

The major goal of this study is to build an improved LFC for a four-area power system network using a superior controller. To achieve excellent performance in dynamic stability, various types of controllers, as reported earlier, were used. The conventional controller was created to tackle these challenges due to the nonlinearity of the power system component utilized in modeling the power system network. The controller in four-area modeling was mostly based on a proportional-integral controller, as the integral gain has the characteristics of both fast-transient recovery and minimal overshoot. The detailed transfer function modeling of intermittent and nonintermittent energy sources of the interconnected hybrid power system is presented in [16, 35].

EVs' demand management technique (DMT) gained popularity in recent years. The development and extensive use of electric vehicles could have a substantial influence on power grids. In this work, a system to model an electric vehicle fleet was devised, and the impact on the load demand of a power system network was investigated. However, it was considered that distinct EV classes' features were not considered. An aggregate model of EV fleets is shown in Figure 1. A deadband function with droop features was included in this model to prevent undesirable frequency fluctuation. ΔF_{UL} and ΔF_{LL} describe the dead band upper and lower limit values, respectively; ΔP_{AG}^{max} and ΔP_{AG}^{min} indicate the maximum and minimum power outputs of the EV fleet, respectively; R_{AG} represents the model droop coefficient (same as conventional units), K_{EV} represents the EV gain, N_{EV} represents the number of connected EVs, T_{EV} represents the battery time constant, and ΔP_{EV} represents the incremental generation change of EV fleet. The transfer function model that describes the effect of the EV fleet is given as follows:

$$G_{EV} = \frac{K_{EV}}{1 + ST_{EV}}. \tag{1}$$

The state equations for all areas for the above interconnected hybrid power system as seen in Figure 2 can be stated as follows:

$$
\begin{aligned}
\dot{\Delta f1} &= \frac{1}{2H_1}\left[-\Delta P_{D1} - \Delta P_{\text{tie},12} - \Delta P_{\text{tie},13} + \Delta P_{md1} + \Delta P_{md5} - \Delta P_{w1} - \Delta P_{\sin v1} - D_1\Delta f_1\right],\\
\dot{\Delta P_{md1}} &= \frac{1}{T_{T1}}\left[\Delta P_{gd1} - \Delta P_{md1}\right],\\
\dot{\Delta P_{md5}} &= \frac{1}{T_{T5}}\left[\Delta P_{gd5} - \Delta P_{md5}\right],\\
\dot{\Delta P_{\sin v1}} &= \frac{1}{T_{inv1}}\left[\Delta P_{s1} - \Delta P_{\sin v1}\right],\\
\dot{\Delta P_{gd1}} &= \frac{1}{T_{g1}}\left[\Delta P_{\text{tie},12} + \Delta P_{\text{tie},13} + \Delta f_1 B_1 - \frac{\Delta f_1}{R_1} - \Delta P_{gd1}\right],\\
\dot{\Delta P_{gd5}} &= \frac{1}{T_b}\left[\Delta P_{\text{tie},12} + \Delta P_{\text{tie},13} + \Delta f_1 B_1 - \Delta P_{gd5}\right],\\
\dot{\Delta P_{EV1}} &= \frac{1}{T_{EV1}}\left[\Delta P_{\text{tie},12} + \Delta P_{\text{tie},13} + \Delta f_1 B_1 - \frac{\Delta f_1}{R_{AG1}} - \Delta P_{EV1}\right],\\
\dot{\Delta f2} &= \frac{1}{2H_2}\left[-\Delta P_{D2} + A_{12}\Delta P_{\text{tie},12} - \Delta P_{\text{tie},24} + \Delta P_{md2} - \Delta P_{w2} - \Delta P_{\sin v2} - D_2\Delta f_2\right],\\
\dot{\Delta P_{md2}} &= \frac{1}{T_{T2}}\left[\Delta P_{gd2} - \Delta P_{md2}\right],\\
\dot{\Delta P_{gd2}} &= \frac{1}{T_{g2}}\left[-A_{12}\Delta P_{\text{tie},12} + \Delta P_{\text{tie},24} + \Delta f_2 B_2 - \frac{\Delta f_2}{R_2} - \Delta P_{gd2}\right],\\
\dot{\Delta P_{\sin v2}} &= \frac{1}{T_{inv2}}\left[\Delta P_{s2} - \Delta P_{\sin v2}\right],\\
\dot{\Delta P_{EV2}} &= \frac{1}{T_{EV2}}\left[-A_{12}\Delta P_{\text{tie},12} + \Delta P_{\text{tie},24} + \Delta f_2 B_2 - \frac{\Delta f_2}{R_{AG2}} - \Delta P_{EV2}\right],\\
\dot{\Delta f3} &= \frac{1}{2H_3}\left[-\Delta P_{D3} + A_{13}\Delta P_{\text{tie},13} - \Delta P_{\text{tie},34} + \Delta P_{md3} - \Delta P_{w3} - \Delta P_{\sin v3} - D_3\Delta f_3\right],\\
\dot{\Delta P_{md3}} &= \frac{1}{T_{T3}}\left[\Delta P_{gd3} - \Delta P_{md3}\right],\\
\dot{\Delta P_{gd3}} &= \frac{1}{T_{g3}}\left[-A_{13}\Delta P_{\text{tie},13} + \Delta P_{\text{tie},34} + \Delta f_3 B_3 - \frac{\Delta f_3}{R_3} - \Delta P_{gd3}\right],\\
\dot{\Delta P_{\sin v3}} &= \frac{1}{T_{inv3}}\left[\Delta P_{s3} - \Delta P_{\sin v3}\right],\\
\dot{\Delta P_{EV3}} &= \frac{1}{T_{EV3}}\left[-A_{13}\Delta P_{\text{tie},13} + \Delta P_{\text{tie},34} + \Delta f_3 B_3 - \frac{\Delta f_3}{R_{AG3}} - \Delta P_{EV3}\right],\\
\dot{\Delta f4} &= \frac{1}{2H_4}\left[-\Delta P_{D4} + A_{34}\Delta P_{\text{tie},34} + A_{24}\Delta P_{\text{tie},24} + \Delta P_{md4} - \Delta P_{w4} - \Delta P_{\sin v4} - D_4\Delta f_4\right],\\
\dot{\Delta P_{md4}} &= \frac{1}{T_{T4}}\left[\Delta P_{gd4} - \Delta P_{md4}\right],\\
\dot{\Delta P_{gd4}} &= \frac{1}{T_{g4}}\left[-A_{34}\Delta P_{\text{tie},34} - A_{24}\Delta P_{\text{tie},24} + \Delta f_4 B_4 - \frac{\Delta f_4}{R_4} - \Delta P_{gd4}\right],\\
\dot{\Delta P_{\sin v4}} &= \frac{1}{T_{inv4}}\left[\Delta P_{s4} - \Delta P_{\sin v4}\right],\\
\dot{\Delta P_{EV4}} &= \frac{1}{T_{EV4}}\left[-A_{34}\Delta P_{\text{tie},34} - A_{24}\Delta P_{\text{tie},24} + \Delta f_4 B_4 - \frac{\Delta f_4}{R_{AG4}} - \Delta P_{EV4}\right].
\end{aligned}
\tag{2}
$$

The state-space equation for the considered system can be expressed as follows:

$$\begin{aligned} \dot{X} &= AX + BU + EW, \\ Y &= CX + DU, \end{aligned} \tag{3}$$

where U is the input variable vector, Y is the output variable vector, X is the state variable vector, and W is the disturbance vector. They are expressed as follows:

$$A = \begin{bmatrix}
\frac{-1}{T_{P1}} & \frac{1}{T_{P1}} & 0 & \frac{-1}{T_{P1}} & 0 & 0 & 0 & 0 & 0 & 0 & 0 & 0 & 0 & 0 & 0 & 0 & 0 & 0 & 0 & 0 & 0 & 0 & 0 & \frac{-1}{T_{P1}} & \frac{-1}{T_{P1}} & 0 & 0 \\
0 & \frac{-1}{T_{T1}} & \frac{1}{T_{T1}} & 0 & 0 & 0 & 0 & 0 & 0 & 0 & 0 & 0 & 0 & 0 & 0 & 0 & 0 & 0 & 0 & 0 & 0 & 0 & 0 & 0 & 0 & 0 & 0 \\
\frac{-1}{R_1 T_{g1}} & 0 & \frac{-1}{T_{g1}} & 0 & 0 & 0 & 0 & 0 & 0 & 0 & 0 & 0 & 0 & 0 & 0 & 0 & 0 & 0 & 0 & 0 & 0 & 0 & 0 & \frac{1}{T_{g1}} & \frac{1}{T_{g1}} & 0 & 0 \\
0 & 0 & 0 & \frac{-1}{T_{inv1}} & 0 & 0 & 0 & 0 & 0 & 0 & 0 & 0 & 0 & 0 & 0 & 0 & 0 & 0 & 0 & 0 & 0 & 0 & 0 & 0 & 0 & 0 & 0 \\
0 & 0 & 0 & 0 & \frac{-1}{T_{T5}} & \frac{1}{T_{T5}} & 0 & 0 & 0 & 0 & 0 & 0 & 0 & 0 & 0 & 0 & 0 & 0 & 0 & 0 & 0 & 0 & 0 & 0 & 0 & 0 & 0 \\
\frac{B_1}{T_b} & 0 & 0 & 0 & 0 & \frac{-1}{T_b} & 0 & 0 & 0 & 0 & 0 & 0 & 0 & 0 & 0 & 0 & 0 & 0 & 0 & 0 & 0 & 0 & 0 & \frac{1}{T_b} & \frac{1}{T_b} & 0 & 0 \\
\frac{-1}{R_{AG1} T_{EV1}} & 0 & \frac{-1}{T_{EV1}} & 0 & 0 & 0 & 0 & 0 & 0 & 0 & 0 & 0 & 0 & 0 & 0 & 0 & 0 & 0 & 0 & 0 & 0 & 0 & 0 & \frac{1}{T_{EV1}} & \frac{1}{T_{EV1}} & 0 & 0 \\
0 & 0 & 0 & 0 & 0 & 0 & 0 & \frac{-1}{T_{P2}} & \frac{1}{T_{P2}} & 0 & \frac{-1}{T_{P2}} & 0 & 0 & 0 & 0 & 0 & 0 & 0 & 0 & 0 & 0 & 0 & 0 & \frac{A_{12}}{T_{P2}} & 0 & \frac{-1}{T_{P2}} & 0 \\
0 & 0 & 0 & 0 & 0 & 0 & 0 & 0 & \frac{-1}{T_{T2}} & \frac{1}{T_{T2}} & 0 & 0 & 0 & 0 & 0 & 0 & 0 & 0 & 0 & 0 & 0 & 0 & 0 & 0 & 0 & 0 & 0 \\
0 & 0 & 0 & 0 & 0 & 0 & 0 & \frac{-1}{R_2 T_{g2}} & 0 & \frac{-1}{T_{g2}} & 0 & 0 & 0 & 0 & 0 & 0 & 0 & 0 & 0 & 0 & 0 & 0 & 0 & \frac{-A_{12}}{T_{g2}} & 0 & \frac{1}{T_{g2}} & 0 \\
0 & 0 & 0 & 0 & 0 & 0 & 0 & 0 & 0 & 0 & \frac{-1}{T_{inv2}} & 0 & 0 & 0 & 0 & 0 & 0 & 0 & 0 & 0 & 0 & 0 & 0 & 0 & 0 & 0 & 0 \\
0 & 0 & 0 & 0 & 0 & 0 & 0 & \frac{-1}{R_{AG2} T_{EV2}} & 0 & \frac{-1}{T_{EV2}} & 0 & 0 & 0 & 0 & 0 & 0 & 0 & 0 & 0 & 0 & 0 & 0 & 0 & \frac{-A_{12}}{T_{EV2}} & 0 & \frac{1}{T_{EV2}} & 0 \\
0 & 0 & 0 & 0 & 0 & 0 & 0 & 0 & 0 & 0 & 0 & \frac{-1}{T_{P3}} & \frac{1}{T_{P3}} & 0 & \frac{-1}{T_{P3}} & 0 & 0 & 0 & 0 & 0 & 0 & 0 & 0 & \frac{A_{13}}{T_{P3}} & 0 & \frac{-1}{T_{P3}} \\
0 & 0 & 0 & 0 & 0 & 0 & 0 & 0 & 0 & 0 & 0 & 0 & \frac{-1}{T_{T3}} & \frac{1}{T_{T3}} & 0 & 0 & 0 & 0 & 0 & 0 & 0 & 0 & 0 & 0 & 0 & 0 & 0 \\
0 & 0 & 0 & 0 & 0 & 0 & 0 & 0 & 0 & 0 & 0 & \frac{-1}{R_3 T_{g3}} & 0 & \frac{-1}{T_{g3}} & 0 & 0 & 0 & 0 & 0 & 0 & 0 & 0 & 0 & \frac{A_{13}}{T_{g3}} & 0 & \frac{1}{T_{g3}} \\
0 & 0 & 0 & 0 & 0 & 0 & 0 & 0 & 0 & 0 & 0 & 0 & 0 & 0 & \frac{-1}{T_{inv3}} & 0 & 0 & 0 & 0 & 0 & 0 & 0 & 0 & 0 & 0 & 0 & 0 \\
0 & 0 & 0 & 0 & 0 & 0 & 0 & 0 & 0 & 0 & 0 & \frac{-1}{R_{AG3} T_{EV3}} & 0 & \frac{-1}{T_{EV3}} & 0 & 0 & 0 & 0 & 0 & 0 & 0 & 0 & 0 & \frac{-A_{13}}{T_{EV3}} & 0 & \frac{1}{T_{EV3}} \\
0 & 0 & 0 & 0 & 0 & 0 & 0 & 0 & 0 & 0 & 0 & 0 & 0 & 0 & 0 & 0 & 0 & \frac{-1}{T_{P4}} & \frac{1}{T_{P4}} & 0 & \frac{-1}{T_{P4}} & 0 & 0 & 0 & \frac{A_{24}}{T_{P4}} & \frac{A_{34}}{T_{P4}} \\
0 & 0 & 0 & 0 & 0 & 0 & 0 & 0 & 0 & 0 & 0 & 0 & 0 & 0 & 0 & 0 & 0 & 0 & \frac{-1}{T_{T4}} & \frac{1}{T_{T4}} & 0 & 0 & 0 & 0 & 0 & 0 \\
0 & 0 & 0 & 0 & 0 & 0 & 0 & 0 & 0 & 0 & 0 & 0 & 0 & 0 & 0 & 0 & 0 & \frac{-1}{R_4 T_{g4}} & 0 & \frac{-1}{T_{g4}} & 0 & 0 & 0 & 0 & \frac{-A_{24}}{T_{g4}} & \frac{-A_{34}}{T_{g4}} \\
0 & 0 & 0 & 0 & 0 & 0 & 0 & 0 & 0 & 0 & 0 & 0 & 0 & 0 & 0 & 0 & 0 & 0 & 0 & 0 & \frac{-1}{T_{inv4}} & 0 & 0 & 0 & 0 & 0 & 0 \\
0 & 0 & 0 & 0 & 0 & 0 & 0 & 0 & 0 & 0 & 0 & 0 & 0 & 0 & 0 & 0 & 0 & \frac{-1}{R_{AG4} T_{EV4}} & 0 & \frac{-1}{T_{EV4}} & 0 & 0 & 0 & 0 & \frac{-A_{24}}{T_{EV4}} & \frac{-A_{34}}{T_{EV4}} \\
2\pi T_{12} & 0 & 0 & 0 & 0 & 0 & 0 & -2\pi T_{12} & 0 & 0 & 0 & 0 & 0 & 0 & 0 & 0 & 0 & 0 & 0 & 0 & 0 & 0 & 0 & 0 & 0 & 0 & 0 \\
2\pi T_{13} & 0 & 0 & 0 & 0 & 0 & 0 & 0 & 0 & 0 & 0 & 0 & -2\pi T_{13} & 0 & 0 & 0 & 0 & 0 & 0 & 0 & 0 & 0 & 0 & 0 & 0 & 0 & 0 \\
0 & 0 & 0 & 0 & 0 & 0 & 0 & 2\pi T_{24} & 0 & 0 & 0 & 0 & 0 & 0 & 0 & 0 & 0 & -2\pi T_{24} & 0 & 0 & 0 & 0 & 0 & 0 & 0 & 0 & 0 \\
0 & 0 & 0 & 0 & 0 & 0 & 0 & 0 & 0 & 0 & 0 & 0 & 2\pi T_{34} & 0 & 0 & 0 & 0 & -2\pi T_{34} & 0 & 0 & 0 & 0 & 0 & 0 & 0 & 0 & 0
\end{bmatrix}, \tag{4}$$

$$x = \begin{bmatrix} \Delta f_1 & \Delta P_{md1} & \Delta P_{gd1} & \Delta P_{sinv1} & \Delta P_{md5} & \Delta P_{gd5} & \Delta P_{EV1} & \Delta f_2 & \Delta P_{md2} & \Delta P_{gd2} & \Delta P_{sinv2} & \Delta P_{EV2} & \Delta f_3 & \Delta P_{md3} & \Delta P_{gd3} & \Delta P_{sinv3} & \Delta P_{EV3} & \Delta f_4 & \Delta P_{md4} & \Delta P_{gd4} & \Delta P_{sinv4} & \Delta P_{EV4} & \Delta P_{tie,12} & \Delta P_{tie,13} & \Delta P_{tie,24} & \Delta P_{tie,34} \end{bmatrix}, \tag{5}$$

$$B = \begin{bmatrix} 0 & 0 & 0 & 0 & 0 \\ 0 & 0 & 0 & 0 & 0 \\ \frac{1}{T_{g1}} & 0 & 0 & 0 & 0 \\ 0 & 0 & 0 & 0 & 0 \\ 0 & 0 & 0 & 0 & 0 \\ 0 & \frac{1}{T_{g5}} & 0 & 0 & 0 \\ 0 & 0 & 0 & 0 & 0 \\ 0 & 0 & 0 & 0 & 0 \\ 0 & 0 & 0 & 0 & 0 \\ 0 & 0 & \frac{1}{T_{g2}} & 0 & 0 \\ 0 & 0 & 0 & 0 & 0 \\ 0 & 0 & 0 & 0 & 0 \\ 0 & 0 & 0 & 0 & 0 \\ 0 & 0 & 0 & 0 & 0 \\ 0 & 0 & 0 & \frac{1}{T_{g3}} & 0 \\ 0 & 0 & 0 & 0 & 0 \\ 0 & 0 & 0 & 0 & 0 \\ 0 & 0 & 0 & 0 & 0 \\ 0 & 0 & 0 & 0 & 0 \\ 0 & 0 & 0 & 0 & \frac{1}{T_{g4}} \\ 0 & 0 & 0 & 0 & 0 \\ 0 & 0 & 0 & 0 & 0 \\ 0 & 0 & 0 & 0 & 0 \\ 0 & 0 & 0 & 0 & 0 \\ 0 & 0 & 0 & 0 & 0 \\ 0 & 0 & 0 & 0 & 0 \end{bmatrix}, \tag{6}$$

$$U = \begin{bmatrix} \Delta P_{g\,d1} & \Delta P_{g\,d5} & \Delta P_{g\,d2} & \Delta P_{g\,d3} & \Delta P_{g\,d4} \end{bmatrix}^{T}, \tag{7}$$

$$E = \begin{bmatrix}
\frac{-1}{T_{P1}} & \frac{-1}{T_{P1}} & 0 & 0 & 0 & 0 & 0 & 0 & 0 & 0 & 0 & 0 & 0 & 0 & 0 & 0 \\
0 & 0 & 0 & 0 & 0 & 0 & 0 & 0 & 0 & 0 & 0 & 0 & 0 & 0 & 0 & 0 \\
0 & 0 & 0 & 0 & 0 & 0 & 0 & 0 & 0 & 0 & 0 & 0 & 0 & 0 & 0 & 0 \\
0 & 0 & \frac{-1}{T_{inv1}} & 0 & 0 & 0 & 0 & 0 & 0 & 0 & 0 & 0 & 0 & 0 & 0 & 0 \\
0 & 0 & 0 & 0 & 0 & 0 & 0 & 0 & 0 & 0 & 0 & 0 & 0 & 0 & 0 & 0 \\
0 & 0 & 0 & 0 & 0 & 0 & 0 & 0 & 0 & 0 & 0 & 0 & 0 & 0 & 0 & 0 \\
0 & 0 & 0 & \frac{-1}{T_{EV1}} & 0 & 0 & 0 & 0 & 0 & 0 & 0 & 0 & 0 & 0 & 0 & 0 \\
0 & 0 & 0 & 0 & \frac{-1}{T_{P2}} & \frac{-1}{T_{P2}} & 0 & 0 & 0 & 0 & 0 & 0 & 0 & 0 & 0 & 0 \\
0 & 0 & 0 & 0 & 0 & 0 & 0 & 0 & 0 & 0 & 0 & 0 & 0 & 0 & 0 & 0 \\
0 & 0 & 0 & 0 & 0 & 0 & 0 & 0 & 0 & 0 & 0 & 0 & 0 & 0 & 0 & 0 \\
0 & 0 & 0 & 0 & 0 & 0 & \frac{-1}{T_{inv2}} & 0 & 0 & 0 & 0 & 0 & 0 & 0 & 0 & 0 \\
0 & 0 & 0 & 0 & 0 & 0 & 0 & \frac{-1}{T_{EV2}} & 0 & 0 & 0 & 0 & 0 & 0 & 0 & 0 \\
0 & 0 & 0 & 0 & 0 & 0 & 0 & 0 & \frac{-1}{T_{P3}} & \frac{-1}{T_{P3}} & 0 & 0 & 0 & 0 & 0 & 0 \\
0 & 0 & 0 & 0 & 0 & 0 & 0 & 0 & 0 & 0 & 0 & 0 & 0 & 0 & 0 & 0 \\
0 & 0 & 0 & 0 & 0 & 0 & 0 & 0 & 0 & 0 & 0 & 0 & 0 & 0 & 0 & 0 \\
0 & 0 & 0 & 0 & 0 & 0 & 0 & 0 & 0 & 0 & \frac{-1}{T_{inv3}} & 0 & 0 & 0 & 0 & 0 \\
0 & 0 & 0 & 0 & 0 & 0 & 0 & 0 & 0 & 0 & 0 & \frac{-1}{T_{EV3}} & 0 & 0 & 0 & 0 \\
0 & 0 & 0 & 0 & 0 & 0 & 0 & 0 & 0 & 0 & 0 & 0 & \frac{-1}{T_{P4}} & \frac{-1}{T_{P4}} & 0 & 0 \\
0 & 0 & 0 & 0 & 0 & 0 & 0 & 0 & 0 & 0 & 0 & 0 & 0 & 0 & 0 & 0 \\
0 & 0 & 0 & 0 & 0 & 0 & 0 & 0 & 0 & 0 & 0 & 0 & 0 & 0 & 0 & 0 \\
0 & 0 & 0 & 0 & 0 & 0 & 0 & 0 & 0 & 0 & 0 & 0 & 0 & 0 & \frac{-1}{T_{inv4}} & 0 \\
0 & 0 & 0 & 0 & 0 & 0 & 0 & 0 & 0 & 0 & 0 & 0 & 0 & 0 & 0 & \frac{-1}{T_{EV4}} \\
0 & 0 & 0 & 0 & 0 & 0 & 0 & 0 & 0 & 0 & 0 & 0 & 0 & 0 & 0 & 0 \\
0 & 0 & 0 & 0 & 0 & 0 & 0 & 0 & 0 & 0 & 0 & 0 & 0 & 0 & 0 & 0 \\
0 & 0 & 0 & 0 & 0 & 0 & 0 & 0 & 0 & 0 & 0 & 0 & 0 & 0 & 0 & 0 \\
0 & 0 & 0 & 0 & 0 & 0 & 0 & 0 & 0 & 0 & 0 & 0 & 0 & 0 & 0 & 0
\end{bmatrix}, \tag{8}$$

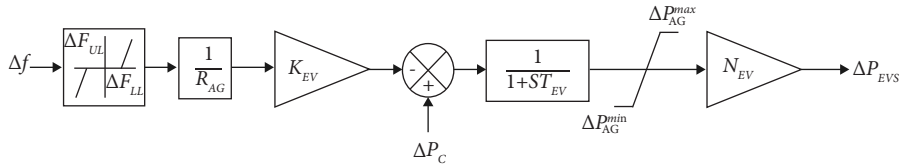

Figure 1: Aggregate model of EV fleets.

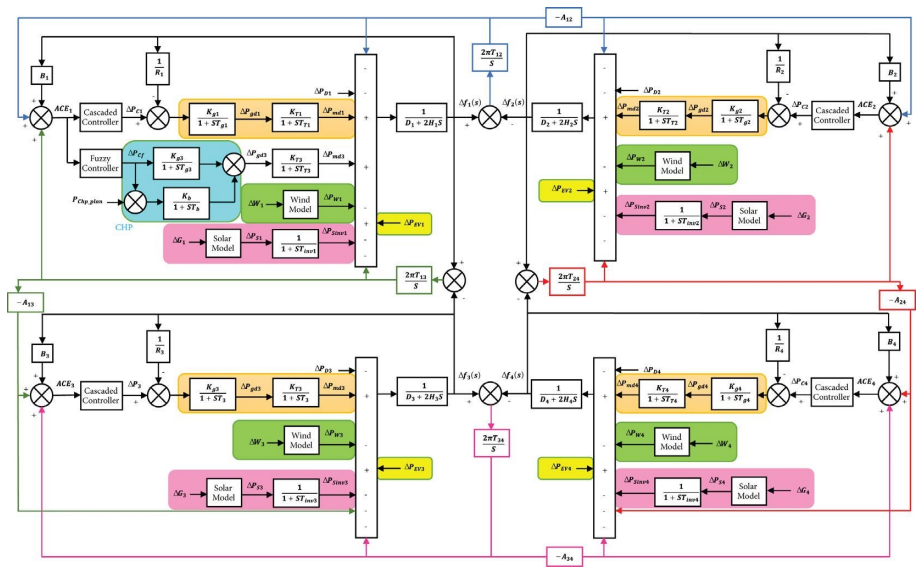

Figure 2: System model of interconnected hybrid power system.

$$W = \left[\, \Delta P_{D1} \;\; \Delta P_{W1} \;\; \Delta P_{S1} \;\; \Delta P_{EV1} \;\; \Delta P_{D2} \;\; \Delta P_{W2} \;\; \Delta P_{S2} \;\; \Delta P_{EV2} \;\; \Delta P_{D3} \;\; \Delta P_{W3} \;\; \Delta P_{S3} \;\; \Delta P_{EV3} \;\; \Delta P_{D4} \;\; \Delta P_{W4} \;\; \Delta P_{EV4} \,\right]^T, \tag{9}$$

$$\mathrm{C} = \begin{bmatrix} 1 & 0 & 0 & 0 & 0 & 0 & 0 & 0 & 0 & 0 & 0 & 0 & 0 & 0 & 0 & 0 & 0 & 0 & 0 & 0 & 0 & 0 & 0 & 0 & 0 & 0 \\ 0 & 0 & 0 & 0 & 0 & 0 & 0 & 1 & 0 & 0 & 0 & 0 & 0 & 0 & 0 & 0 & 0 & 0 & 0 & 0 & 0 & 0 & 0 & 0 & 0 & 0 \\ 0 & 0 & 0 & 0 & 0 & 0 & 0 & 0 & 0 & 0 & 0 & 0 & 1 & 0 & 0 & 0 & 0 & 0 & 0 & 0 & 0 & 0 & 0 & 0 & 0 & 0 \\ 0 & 0 & 0 & 0 & 0 & 0 & 0 & 0 & 0 & 0 & 0 & 0 & 0 & 0 & 0 & 0 & 0 & 1 & 0 & 0 & 0 & 0 & 0 & 0 & 0 & 0 \end{bmatrix}, \tag{10}$$

$$D = 0. \tag{11}$$

3. Proposed Methodology

3.1. LSTM Network. An RNN is a type of artificial neural network that takes advantage of time information in input data, as opposed to a regular neural network that merely has interactions between layers. As a result, RNN performs better when dealing with time-series learning problems. The structure of the LSTM cell includes the input gate, forget gate, and output gate.

The LSTM defines and maintains the cell state to manage information flow, which is an essential factor in the LSTM architecture, to acquire long-term temporal functional relationships [44]. Relying on the results of prior stages and inputs of the current time step, the memory cell state C_{t-1} interacts with the intermediate output h_{t-1} and the succeeding input x_t to determine which parts of the internal state vector should be modified, retained, or discarded. The following are the compact expression of an LSTM network with a forget gate:

$$\begin{aligned} i_t &= \sigma\left(x_t U^i + h_{t-1} W^i\right), \\ f_t &= \sigma\left(x_t U^f + h_{t-1} W^f\right), \\ o_t &= \sigma\left(x_t U^o + h_{t-1} W^o\right), \\ \widetilde{C}_t &= \sigma\left(x_t U^g + h_{t-1} W^g\right), \\ C_t &= f_t * C_{t-1} + i_t * \widetilde{C}_t, \\ h_t &= \tan h\left(C_t\right) * o_t, \end{aligned} \tag{12}$$

where i denotes the input gate; f denotes the forget gate; o denotes the output gate; σ denotes the sigmoid activation function; the operator $*$ denotes element-wise

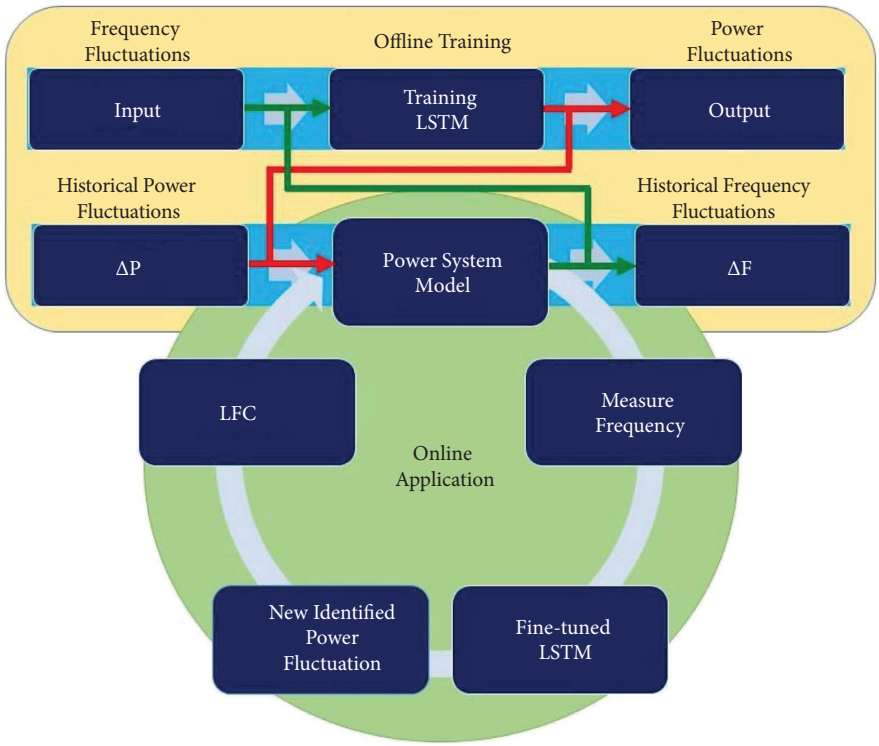

Figure 3: Offline training and online application of the LSTM.

Get the non-intermittent & intermittent generation data and also the non-flexible & flexible (such as EV) load data
Perform the load flow for each time interval
Check the frequency deviation.
If Δ>f 0.5 (because of some unexpected drop in load) then
Check the inequality constraints
If it violates the inequality constraints ($P_i < P_{min,i}$)
Run the FA/FPA algorithm to find the optimal flexible demand with a time limit
End if
End If.
End For
Calculate the system optimal cost function.

Figure 4: Implementation logic of the DMT-coordinated LFC.

multiplication; W^i, W^f, W^o, and W^g denote the weight matrices that need to be learned during training; U^i, U^f, U^o, and U^g are coefficient matrixes; $\tilde{C}_t$ is a "candidate" hidden state, which is calculated based on the current input and the previous hidden state; C_t is the internal memory of the unit, and h_t represents the final output of the memory unit.

LSTM memory units can record sophisticated correlation patterns inside time-series data in both short and long term through the function of different gates, which is a significant advance over other RNNs.

3.2. LSTM Network for Power Identification. The LSTM RNN is used in this work to present an active identification approach for real power perturbations. This provides a new realistic reference for automatic generation control (AGC) to preserve system frequency. The proposed technique is divided into two parts: offline training and online application of the LSTM, with the entire procedure being depicted in Figure 3.

3.2.1. Offline Training Progress. The statistical data of frequency variations, which provides the input for the LSTM training, can be considered the preceding information. The target (i.e., the output) is the real power fluctuation. The training processes are as follows:

(i) Step 1: data on the frequency and active power fluctuations should be collected.

(ii) Step 2: initialize weight matrices and bias vectors, including W^i, W^f, W^o, W^g, U^i, U^f, U^o, and U^g after normalizing data.

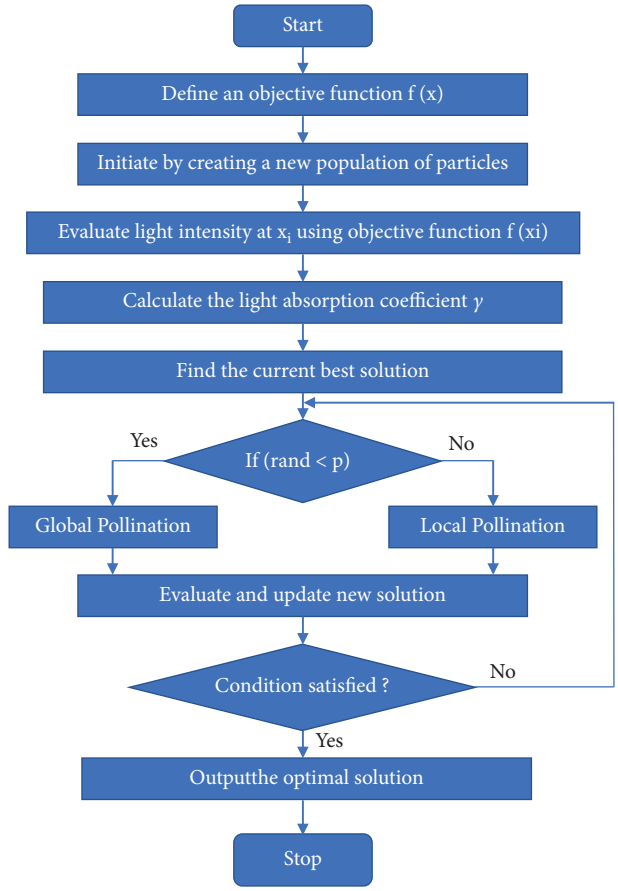

Figure 5: Flowchart that describes the work using FA/FPA algorithm.

Describe an objective function f (x) for minimization problem
Initiate by creating a new population of particles in search space. x_i *(i=1, 2..n)*
The objective function f (x_i*) evaluates light intensityat* x_i*.*
Calculate the light absorption coefficient γ*.*
Obtain a switch probability whose value is distributed uniformly.
While (t < Max generation)
  for a=1:1:n
    for b=1:1:i
      if ($I_a > I_b$)
        Lesser brighter particle a move towards the brighter particle b.
          If (rand < p)
            The attraction between the fireflies (β*) varies with distance r. (exp (-*γr^2*))*
            Do Global walk through
              $x_a^{k+1} = x_a^k + (\beta / r) * (x_b^k - x_a^k) * (r * (\mathrm{rt})^2 - tmpf)$
              where $tmpf = \alpha * (r1 - (1/2)) * scale$
            else
            Do Global walk through
            $x_a^{k+1} = x_a^k + ((x_b^k - x_a^k) * (rand)^2)$
            end if
          end if
          Evaluate and update new solutions.
        end for b: for all agents
      end for a: for all agents
Set the agents' positions by ranking them, and then get the current global best particle.

Figure 6: Implementation logic of the FA/FPA algorithm.

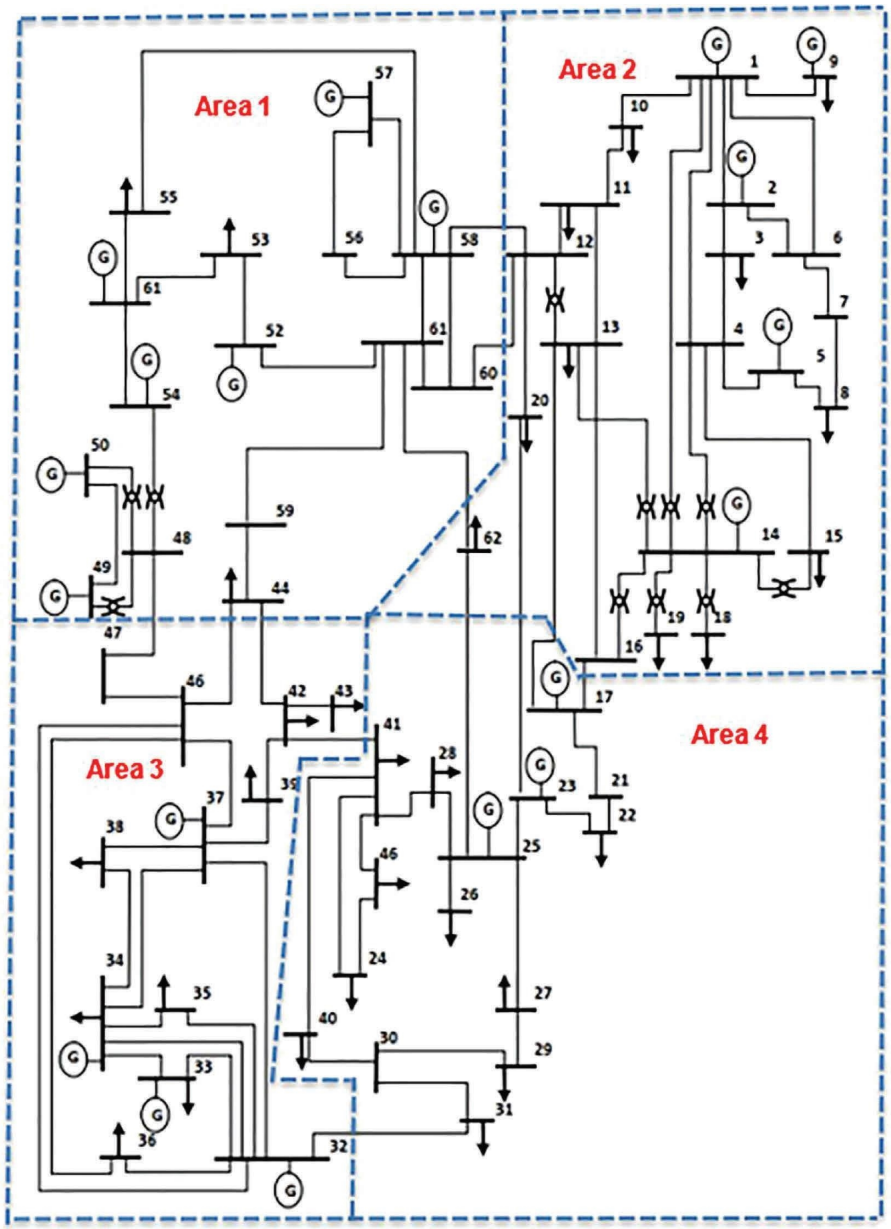

Figure 7: 62 bus Indian utility system.

(iii) Step 3: by updating the weight coefficients and bias vectors, the neural network is trained using the backward propagation approach with the gradient-based optimizer to minimize the cost function.

(iv) Step 4: invert the recognized power fluctuations from the normalized to real values, then output the results of the identification.

3.2.2. Online Application. The proposed LSTM network is trained using previous data in the offline environment and created using power and frequency changes. Once the LSTM network is properly trained, it may be used online to calculate power fluctuations based on the frequency observed online. It is worth noting that varied system running conditions can be considered for training database development when in the offline training mode. In addition, the model can be updated on a regular basis if fresh online measurement and generated data becomes available, or if the system's conditions change unexpectedly. Frequency control resources, such as synchronous generators and ESSs, clear out all the recognized real-time power perturbations and form a control signal for AGC.

3.2.3. Performance Evaluation. To assess the identification accuracy of the proposed LSTM RNN methodology, the Integral Time Absolute Error (ITAE) is considered as the performance index. Compared to other performance indices such as Integral Squared Error (ISE), Integral Absolute Error (IAE), and Integral Time-Weighted-Squared Error (ITSE), ITAE performs well in the fine-tuning of PID controller

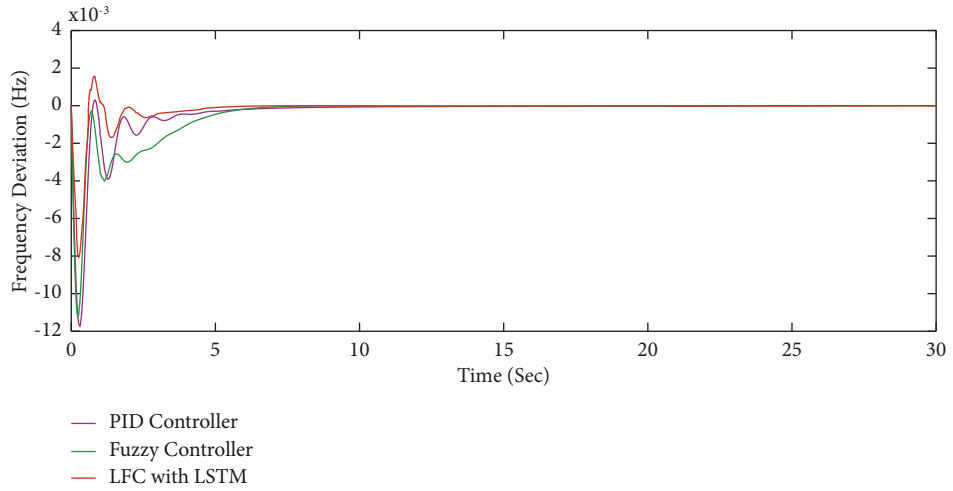

Figure 8: Case 01—Frequency Deviation for area 1.

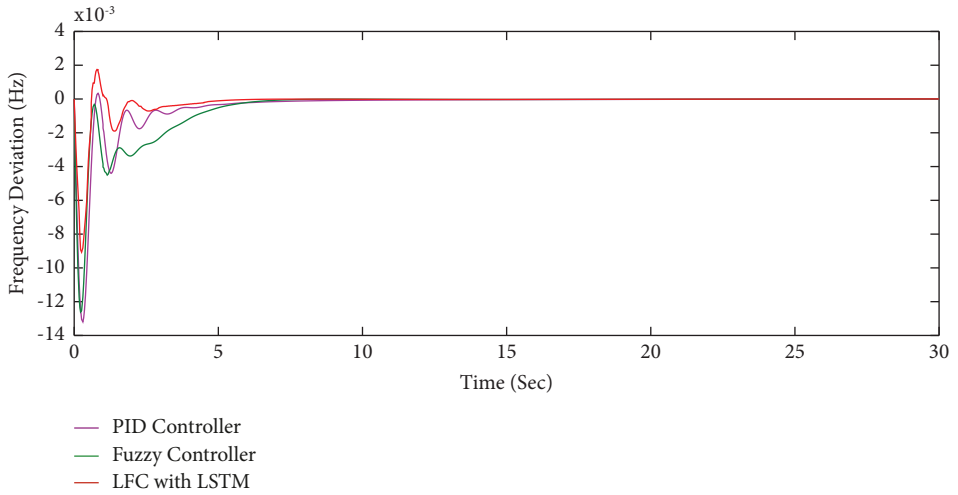

Figure 9: Case 01—Frequency Deviation for area 2.

gains due to lesser overshoots/undershoots and fluctuations [10]. Equations (14)–(17) describe the fitness function of ITAE and the PID controller gain limits, respectively. By optimizing the fitness function of ITAE, the PID controller gains are well-tuned.

For area-n,

$$u_n = K_{pn}ACE_n + K_{in}\int_0^t ACE_n \mathrm{d}t + K_{dn}\frac{dACE_n}{\mathrm{d}t}, \tag{13}$$

$$\text{Fitness Function} = \text{Minimize}\{\text{ITAE}\} = \int_0^t \{|ACE_n|\}\mathrm{d}t = \int_0^t \left\{\left(|\Delta F_n| + \left|\Delta P_{\text{tie},n-j}\right|\right)\right\}\mathrm{d}t. \tag{14}$$

Subjected to PID gain limits,

$$K_{pj}^{\min} \le K_{pj} \le K_{pj}^{\max}, \tag{15}$$

$$K_{ij}^{\min} \le K_{ij} \le K_{ij}^{\max}, \tag{16}$$

$$K_{dj}^{\min} \le K_{dj} \le K_{dj}^{\max}, \tag{17}$$

where n denotes the number of areas; $j = 1, 2, \ldots n (j \neq n)$; ΔF_n denotes the frequency deviations in the n^{th} area; $\Delta P_{\text{tie},n-j}$ denotes the tie line power fluctuation.

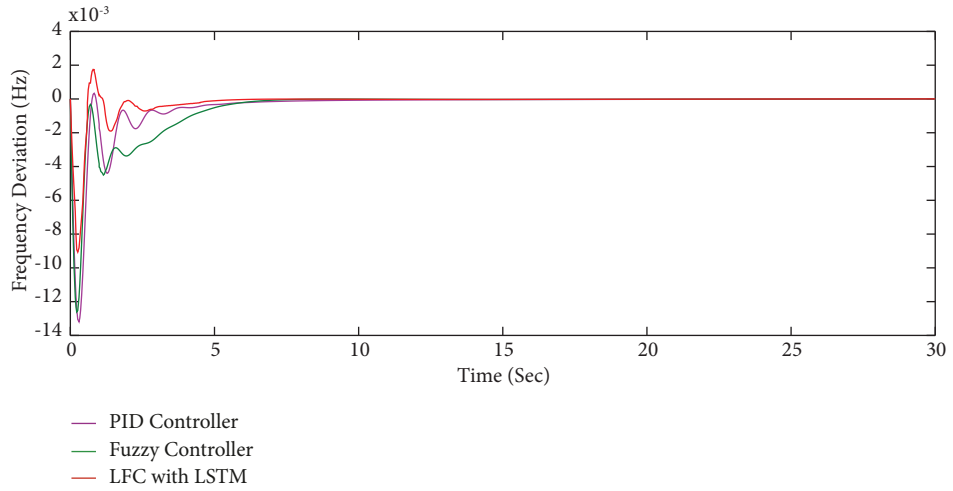

Figure 10: Case 01—Frequency Deviation for area 3.

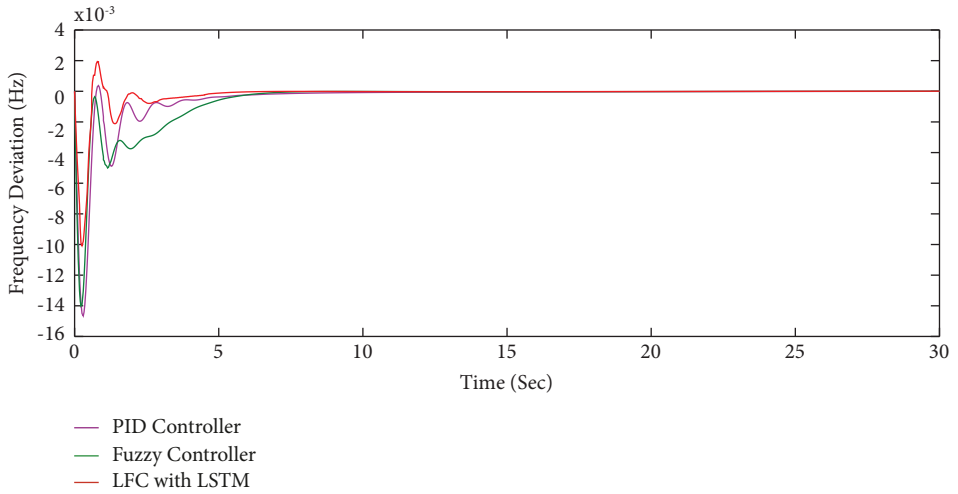

Figure 11: Case 01—Frequency Deviation for area 4.

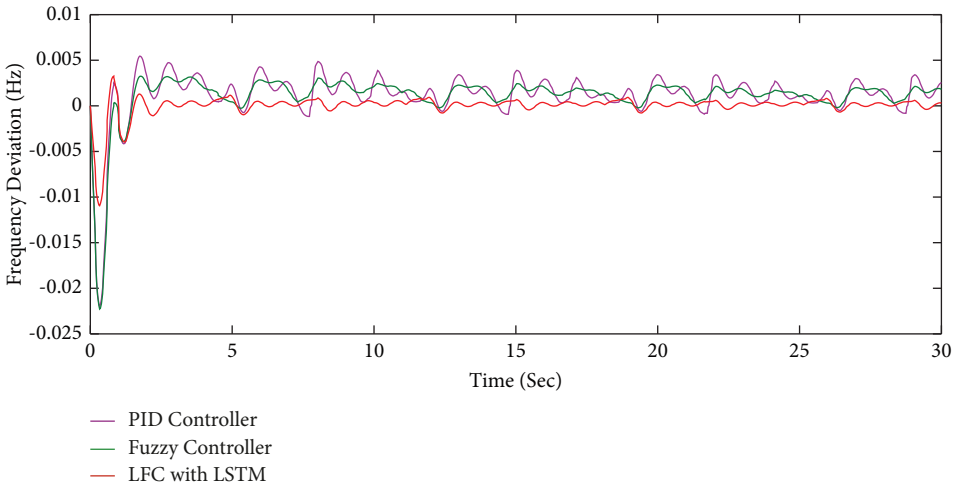

Figure 12: Case 02—Frequency Deviation for area 1.

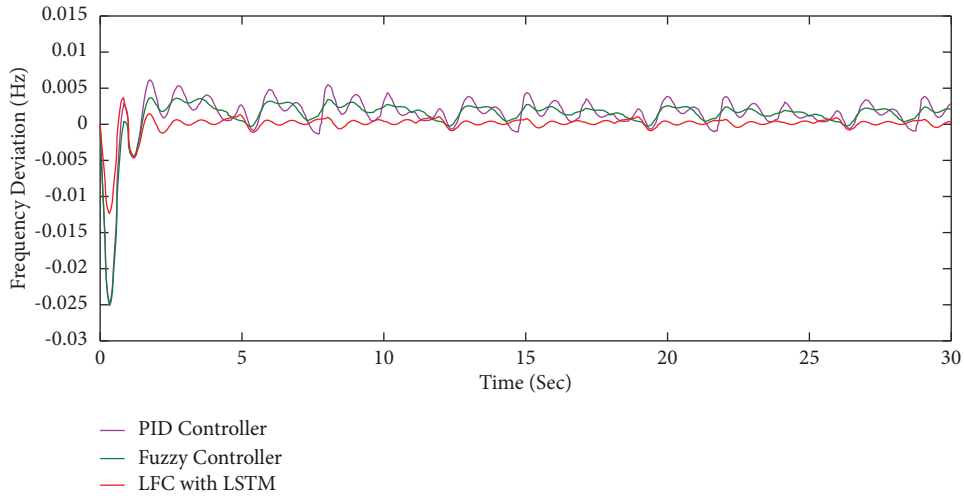

Figure 13: Case 02—Frequency Deviation for area 2.

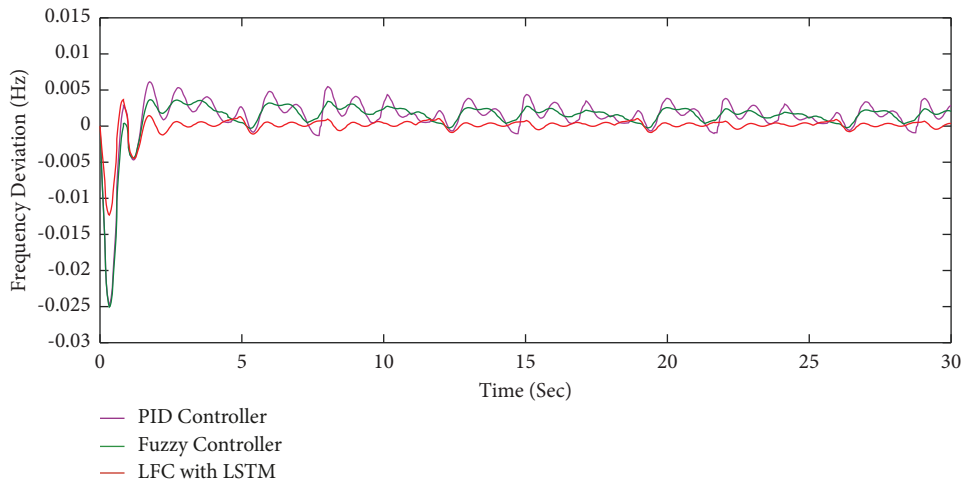

Figure 14: Case 02—Frequency Deviation for area 3.

3.2.4. Demand Management Technique. The primary goal of the DMT is to reduce system peak demand and its operational cost. In this considered work, the clipping of system peak demand can be achieved with the help of the working behavior of EVs while the system operational cost can be managed with the help of nonintermittent power generation units such as thermal units and combined heat and power generation units. The formulation of the objective function with their constraints is listed as follows:

$$\text{Minimize}\left[\frac{\Delta V_{\min,i}}{\Delta P_d}+\sum_{i=1}^{N_p}C_i\left(P_i^p\right)+\sum_{j=1}^{N_c}C_j\left(P_j{}^c,H_j{}^c\right)\right], \quad (18)$$

where $\Delta V_{\min,i}$ is the variation in minimum voltage, P_d is the variation in electrical power demand, N_p and N_c represent the number of conventional thermal and cogeneration units, respectively, $C_i(P_i^p)$ represents the fuel cost of the conventional thermal units, and $C_j(P_j{}^c, H_j{}^c)$ represents the fuel cost of the cogeneration units and they are expressed as follows:

$$\begin{aligned}C_i\left(P_i^p\right)&=\alpha_i\left(P_i{}^p\right)^2+\beta_i\left(P_i{}^p\right)+\gamma_i,\\ C_j\left(P_j{}^c,H_j{}^c\right)&=a_j\left(P_j{}^c\right)^2+b_j\left(P_j{}^c\right)+c_j.\end{aligned} \quad (19)$$

Subject to the following constraints,

$$\begin{aligned}\sum_{i=1}^{N_p}P_i{}^p+\sum_{j=1}^{N_c}P_j{}^c&=P_d,\\ P_i{}^{p_{\min}}\le P_i{}^p\le P_i{}^{p_{\max}}&\text{ where }\quad i=1,2\ldots N_p,\\ P_j{}^{c_{\min}}\left(H_j{}^c\right)\le P_j{}^c\le P_j{}^{c_{\max}}\left(H_j{}^c\right)&\text{ where }\quad j=1,2\ldots N_c.\end{aligned} \quad (20)$$

The operation of the suggested DMT is to determine the best timings for charging electric vehicles and turning on various heating loads while adhering to the aforementioned restrictions [45, 46]. To keep frequency oscillation to the minimum, the considered system fully relies on the nonintermittent power generation units. However, it is also

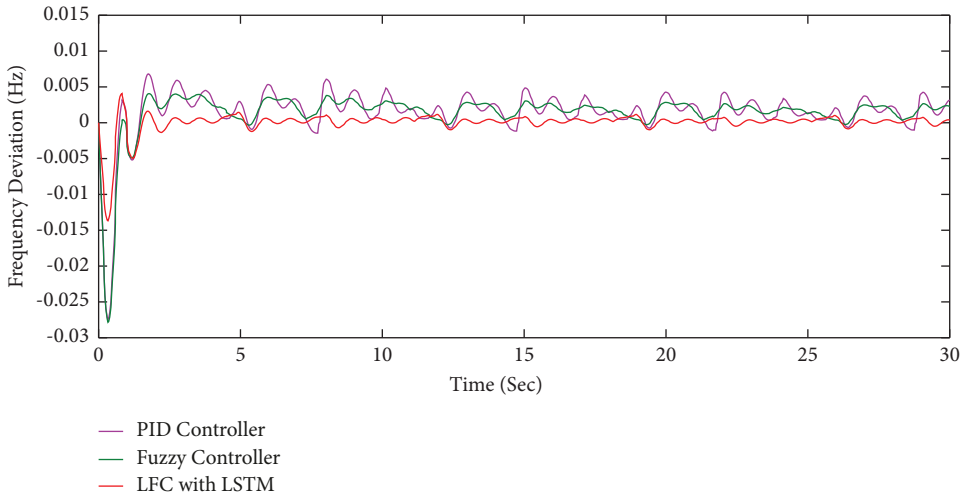

Figure 15: Case 02—Frequency Deviation for area 4.

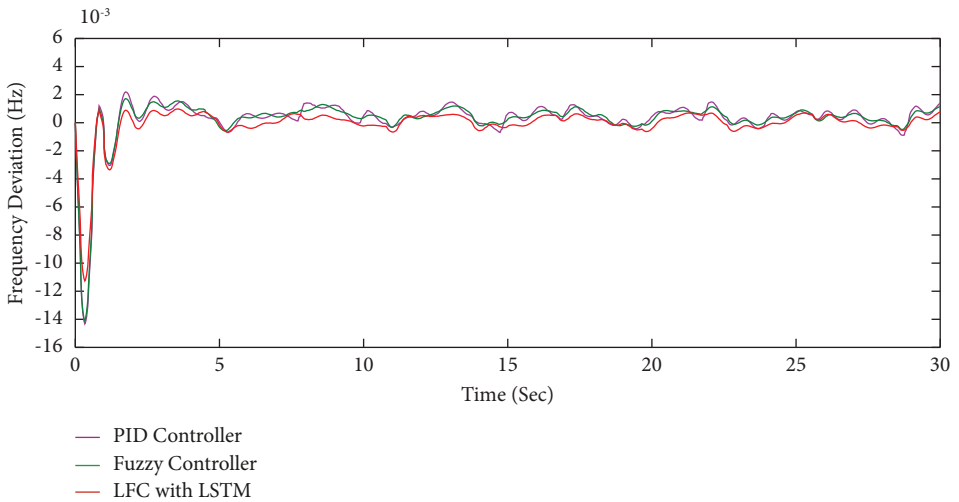

Figure 16: Case 03—Frequency Deviation for area 1.

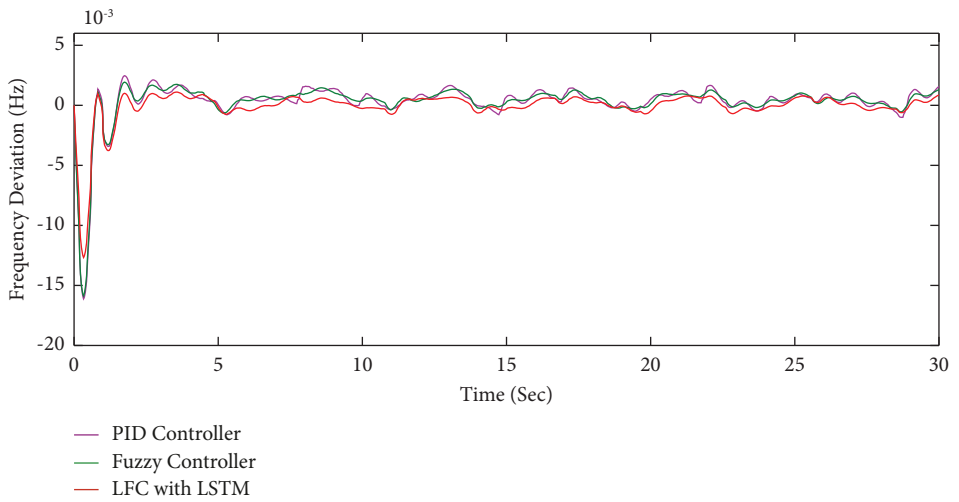

Figure 17: Case 03—Frequency Deviation for area 2.

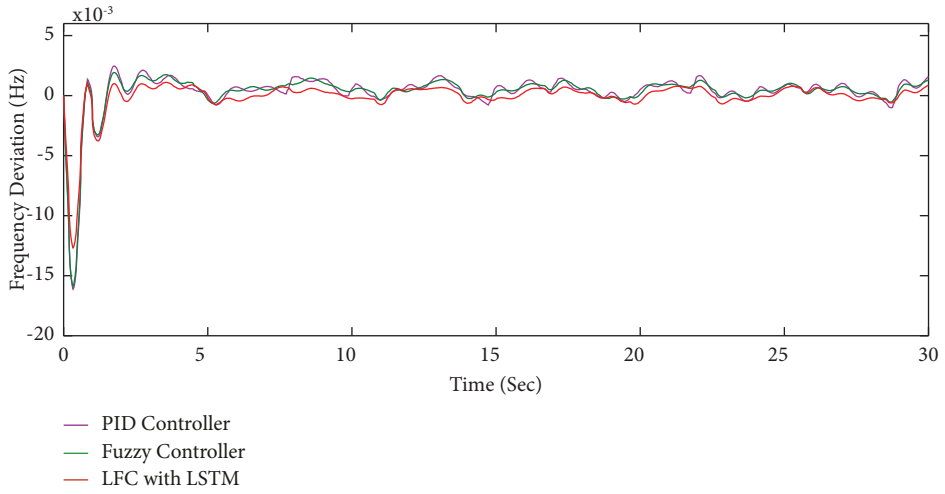

Figure 18: Case 03—Frequency Deviation for area 3.

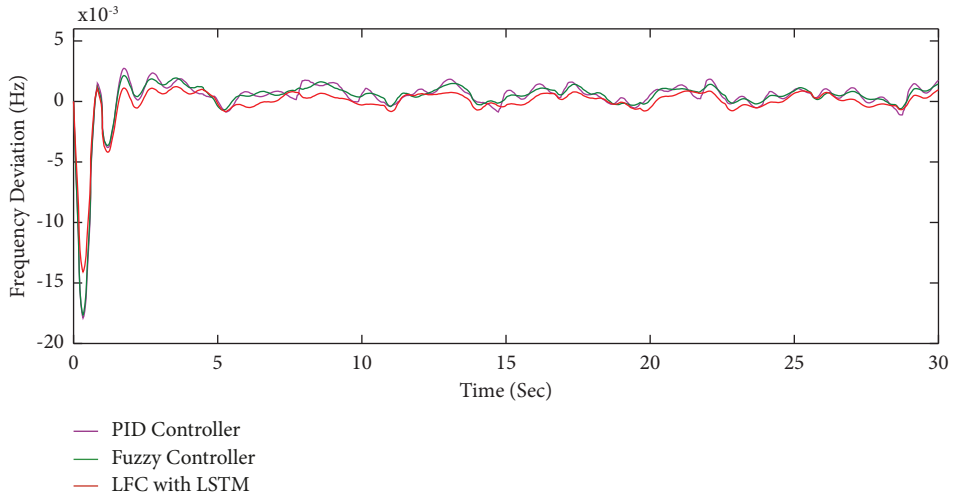

Figure 19: Case 03—Frequency Deviation for area 4.

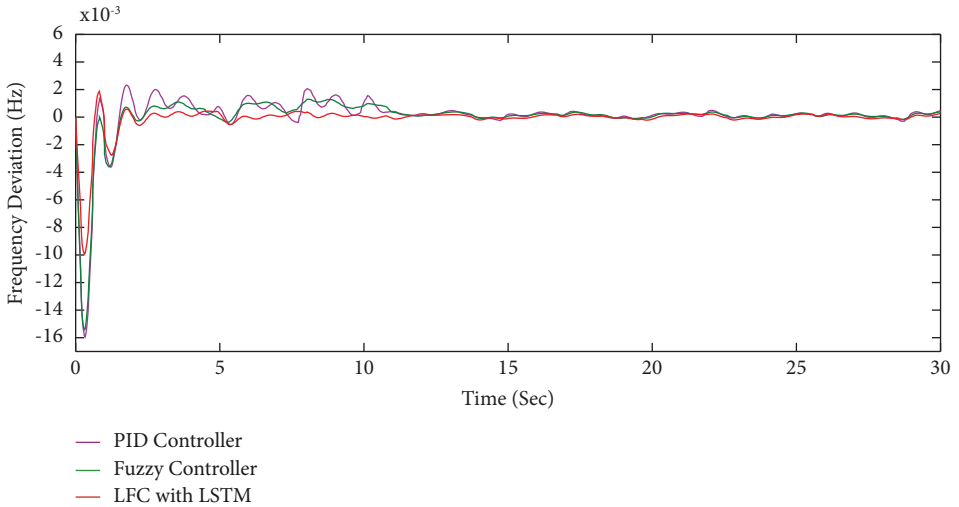

Figure 20: Case 04—Frequency Deviation for area 1.

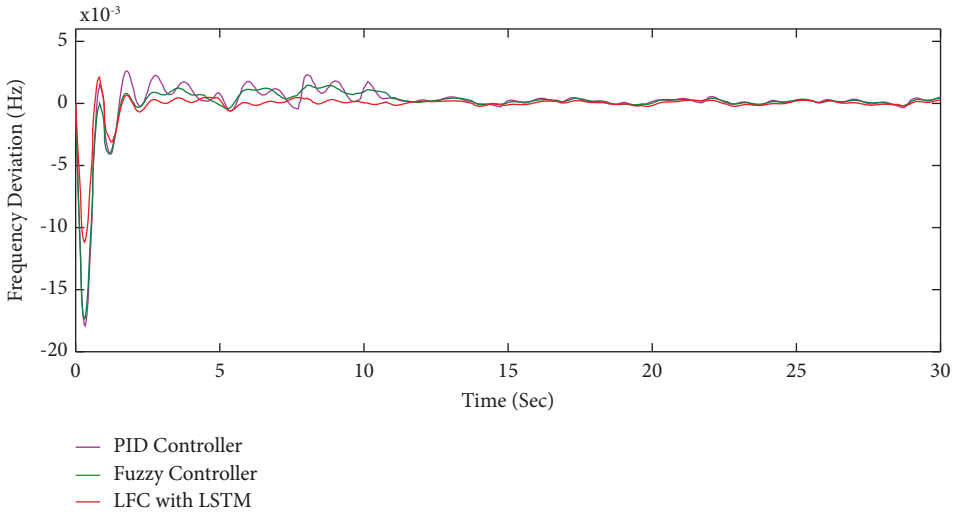

Figure 21: Case 04—Frequency Deviation for area 2.

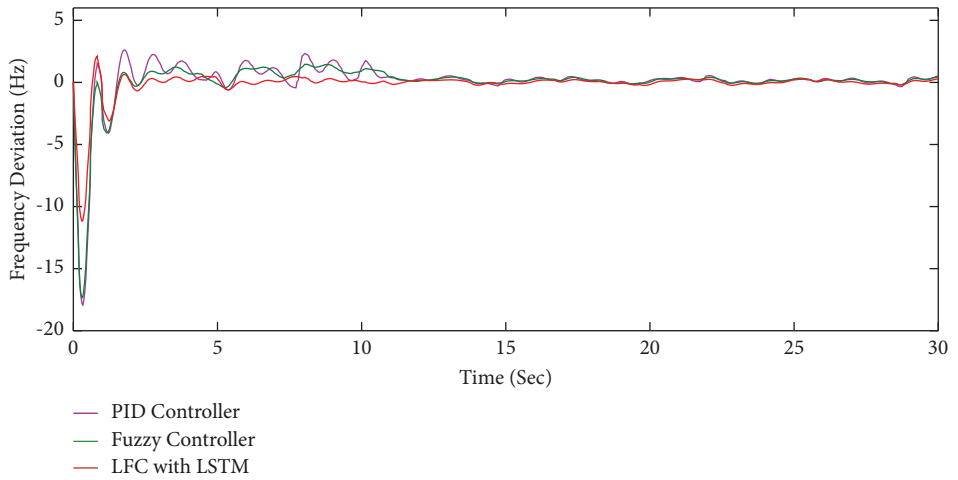

Figure 22: Case 04—Frequency Deviation for area 3.

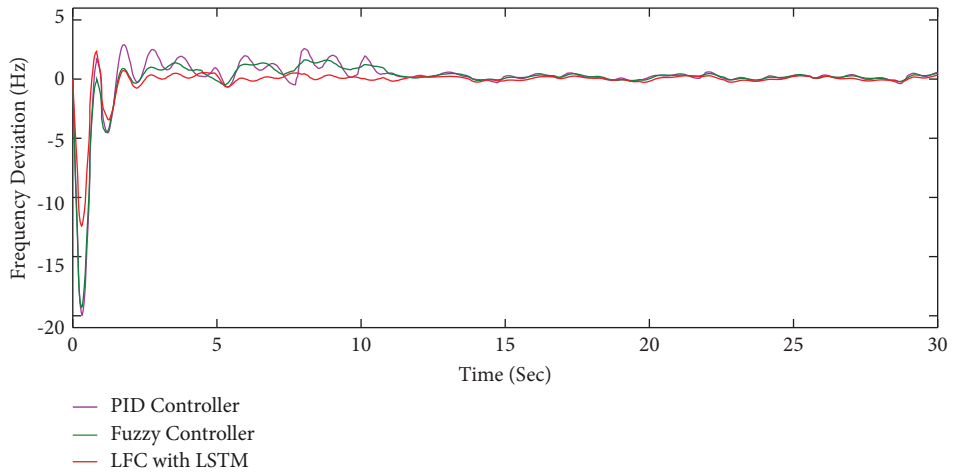

Figure 23: Case 04—Frequency Deviation for area 4.

limited by their upper and lower bounds. Therefore, in such a scenario, the FA/FPA algorithm can be used to find the optimal flexible demand, which will reduce the system operation cost and ensure standard system frequency. The implementation logic of the DMT coordinated LFC is described in Figure 4.

The system frequency rises due to an unexpected drop in load. Nonintermittent power generation must be altered to achieve zero frequency variation. In some unconditional situations, this cannot be performed beyond a certain limit as it will further increase the system's operational cost due to the temporary shutdown and startup. Then, given a time constraint, the FA/FPA algorithm is run to determine optimum flexible demand, which can then be introduced to the system to satisfy zero frequency deviation and to calculate the optimal cost function.

4. FA/FPA Algorithm

The proposed technique is based on two metaheuristic algorithms, Firefly Algorithm and Flower Pollination Algorithm, which were thoroughly examined in this research work. These proposed algorithms combine the concepts of exploration (diversification) and exploitation (intensification) to create a hybrid algorithm. Exploration is a global search term, while exploitation is a local search term. The Firefly Algorithm (FA) is based on the blinking characteristic of fireflies, which are influenced by their natural behavior and bioluminescence phenomena. These fireflies move toward an attractive firefly that serves as the present global best. Optimization is used to determine the flashing brightness of fireflies.

The Flower Pollination Algorithm (FPA) is based on the properties of the flowers of various plants. The main goal is to reproduce by transferring pollen and pollinators such as insects, birds, bees, and flies assist in this process. Abiotic (self-pollination) and biotic (cross-pollination) pollination are the different sorts of pollination. As pollinators travel a great distance, global pollination (biotic) happens over vast distances. Cross-pollination occurs within flowers of the same plant. To reach speedier optimums, both processes are regulated by a switch probability p.

Both FA and FPA algorithms employ biological notions. The fundamental goal of hybridization is to solve the drawbacks of existing separate optimization algorithm components and generate a better form. Second, to establish the robustness of this suggested algorithm in terms of achieving global optima in very little time while maximizing the utilization of the exploration and exploitation concepts. Both these concepts are used to investigate new potential outcomes as well as improve the current solution. The flowchart that describes the considered work using FA/FPA is shown in Figure 5.

The suggested algorithm introduces both concepts. The movement of particles in this method is based on moving less brighter particles toward brighter ones by completing local and global walks in two phases, identical to the Firefly Algorithm and Flower Pollination Algorithm. The FA/FPA algorithm incorporates the Firefly Algorithm concept by first

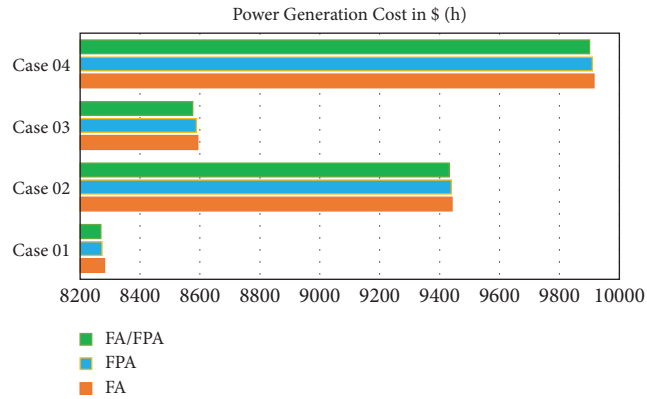

Figure 24: Power generation cost comparison for all cases.

opting for a local search as all particles are divided into numerous subgroups and then selecting the best value from each group. By preventing from being trapped within local optima and reducing the randomness effect, they were able to find a global best one value from all these values, allowing particles to explore a better optima solution. As a result, the entire process includes the global step, which is efficiently completed by the particles. The suggested algorithm (FA/FPA) then uses the Flower Pollination Algorithm paradigm to create an interaction between local and global search. This results in a switch probability having a magnitude bigger than the random number generation of particles, as the particles can move in any direction in a local walk and hence the effect of randomization is greater.

The exploitation impact is included in the local search of the Flower Pollination Algorithm because flowers of the same species are selected using the flower consistency process, and pollen transfer occurs in the same plant. Similarly, the proposed algorithm's local search exploits particles belonging to the same species. As a result, the convergence rate is quicker as particles will do a more efficient local search. In the considered work, the minimum system operational cost can be taken as the objective function, which can be achieved with the application of FA/FPA. The implementation logic of the FA/FPA can be described as a pseudocode in Figure 6.

5. Simulation Results and Discussion

Due to the significant penetration of intermittent power generation and variable flexible loads, the frequency stability of an Indian power system is challenged. The one-line diagram of the typical 62-bus Indian utility system is shown in Figure 7 and their corresponding generator data is shown in Table 1. The area-wise number of both intermittent and nonintermittent power generation units is provided in [47]. The four-area power system is modeled using MATLAB/Simulink tools, which includes the effects of renewable energy sources and electric vehicles. This four-area power system is linked to the proposed controller, which has been put through its paces under various operating situations to test the efficiency of the controller's response. The test system is simulated in four different scenarios, and the

Table 1: Generator data of 62 bus Indian utility system.

Gen. No.	$P_{i,min}$(MW)	$P_{i,max}$ MW	a_i (CU/(MWhr)^2)	b_i (CU/MWhr)	c_i (CU/hr)	Bus no	Voltage mag.	Angle deg.	MW	Mvar	Q_{min}	Q_{max}	Area
G_1	50	300	0.0070	6.80	95	1	1.05	0	192.64	23.55	0	450	2
G_2	50	450	0.0055	4.00	30	2	1.05	0	190.58	0.00	0	130	2
G_3	50	450	0.0055	4.00	45	5	1.05	0	255.68	0.00	0	255	2
G_4	0	150	0.0025	0.85	10	9	1.05	0	78.202	1.218	0	100	2
G_5	50	300	0.0060	4.60	20	14	1.05	0	171.08	233.9	0	500	2
G_6	50	450	0.0055	4.00	90	17	1.05	0	190.61	0.00	0	0	4
G_7	50	200	0.0065	4.70	42	23	1.05	0	151.84	147.9	0	340	4
G_8	50	500	0.0075	5.00	46	25	1.05	0	250.24	86.52	0	395	4
G_9	0	600	0.0085	6.00	55	32	1.05	0	106.62	0.00	−100	400	3
G_{10}	0	100	0.0020	0.50	58	33	1.05	0	62.380	0.00	0	30	3
G_{11}	50	150	0.0045	1.60	65	34	1.05	0	134.50	41	0	41	3
G_{12}	0	100	0.0025	0.85	78	37	1.05	0	78.533	0.00	0	87	3
G_{13}	50	300	0.0050	1.80	75	49	1.05	0	213.95	0.00	0	80	1
G_{14}	0	150	0.0045	1.60	85	50	1.05	0	92.784	0.00	0	200	1
G_{15}	0	500	0.0065	4.70	80	51	1.05	0	82.957	41.54	0	245	1
G_{16}	50	150	0.0045	1.40	90	52	1.05	0	24.608	35	0	35	1
G_{17}	0	100	0.0025	0.85	10	54	1.05	0	72.633	0.00	0	100	1
G_{18}	50	300	0.0045	1.60	25	57	1.05	0	219.44	0.00	0	20	1
G_{19}	100	600	0.0080	5.50	90	58	1.05	0	339.70	100	100	420	1

suggested controller response is compared to that of a standard PID controller and a fuzzy controller.

5.1. Case 01 (System Response with All Energy Resources). Case 01 deals with intermittent and nonintermittent power generation in all four areas. Figures 8–11 show the simulation of the system's reaction with a load variation of 0.01 p.u and the accompanying responses associated with the suggested controller, which delivers a superior and faster response when compared to traditional PID and fuzzy controllers. Moreover, better frequency response is required to reduce associated power generation cost. Nonintermittent power generation units in each of the four zones are responsible for this.

5.2. Case 02 (System Response with Change of ΔP_w). For frequency regulation with the effects of wind power, Case 02 considers both intermittent and nonintermittent power generation in the four areas under study. Variations in solar power and load are retained as constant, whereas only variations in wind power are implemented with rising and falling ΔP_w values. As wind power is an intermittent power source, it is frequently encountered in the power system. Figures 12–15 present the findings of the system response using the proposed controller to handle these variations in ΔP_w values. Compared to PID and fuzzy controllers, frequency deviation provides a better and faster reaction while minimizing power generation costs with good frequency response, meeting the frequency deviation within ±0.5 when using the FA/FPA algorithm.

5.3. Case 03 (System Response with Change of ΔP_S). For frequency regulation with the effects of solar power, Case 03 considers both intermittent and nonintermittent power generation in the four areas under study. Only variations in solar power are implemented with a rise in the value of ΔP_S, while variations in wind power and load remain constant. As solar power is an intermittent power source, it is frequently encountered in the power system. Figures 16–19 present the findings of the system response using the proposed controller to handle variations in ΔP_S values. To maintain better frequency response, control inputs to nonintermittent power generation units such as thermal, and CHP are modified in a decreasing manner when solar power increases. Simultaneously, the suggested FA/FPA algorithm reduces power-generating costs by improving frequency response and achieving a frequency deviation of less than ±0.5.

5.4. Case 04 (System Response with Change of ΔP_L, ΔP_W, and ΔP_S). Case 04 considers both intermittent and nonintermittent power generation in all four areas for load frequency regulation with all conceivable system disturbances. This case connects the problems discussed in the three earlier cases at the same time. If changes in solar and wind power are accompanied by increases in the values of ΔP_S and ΔP_W, and changes in load value are accompanied by decreases in the value of ΔP_L, then the nonintermittent power generation units must be modified to suit the power demand while still being within their constraints to keep the frequency deviation (+0.5) within a limit. If the nonintermittent power generation units fail to match the above criteria, the FA/FPA algorithm-based DMT can be used to determine the best flexible demand (such as electric vehicle charging) with a time constraint, which can then be incorporated to achieve zero frequency deviation. Figures 20–23 present the findings of the system response using the suggested controller to handle these changes in ΔP_L, ΔP_W, and ΔP_S. The frequency deviation of the system for the proposed controller is superior in maintaining almost

Table 2: Performance measures of Proposed Controller.

S. No	Case	Area	Parameter	PID controller	Fuzzy controller	Proposed controller
1.	Case 01	Area 01	|Peak Mag| (Hz)	0.0117	0.0112	0.0080
			Settling time (sec)	18.44	8.08	6.38
		Area 02	|Peak Mag| (Hz)	0.0133	0.0127	0.0091
			Settling time (sec)	17.84	8.31	6.65
		Area 03	|Peak Mag| (Hz)	0.0131	0.0126	0.0089
			Settling time (sec)	17.98	8.38	6.72
		Area 04	|Peak Mag| (Hz)	0.0147	0.0140	0.0100
			Settling time (sec)	13.44	8.52	6.80
2.	Case 02	Area 01	|Peak Mag| (Hz)	0.0222	0.0219	0.0109
			Settling time (sec)	67.88	59.37	48.36
		Area 02	|Peak Mag| (Hz)	0.0251	0.0248	0.0124
			Settling time (sec)	70.34	60.86	49.28
		Area 03	|Peak Mag| (Hz)	0.0250	0.0246	0.0122
			Settling time (sec)	70.82	60.50	48.88
		Area 04	|Peak Mag| (Hz)	0.0279	0.0274	0.0137
			Settling time (sec)	69.46	61.45	48.14
3.	Case 03	Area 01	|Peak Mag| (Hz)	0.0143	0.0141	0.0112
			Settling time (sec)	57.88	49.37	38.36
		Area 02	|Peak Mag| (Hz)	0.0162	0.0159	0.0127
			Settling time (sec)	60.34	50.86	39.28
		Area 03	|Peak Mag| (Hz)	0.0160	0.0157	0.0126
			Settling time (sec)	60.82	50.50	38.88
		Area 04	|Peak Mag| (Hz)	0.0179	0.0176	0.0140
			Settling time (sec)	59.46	51.45	38.14
4.	Case 04	Area 01	|Peak Mag| (Hz)	0.0159	0.0154	0.0099
			Settling time (sec)	47.12	43.87	36.12
		Area 02	|Peak Mag| (Hz)	0.0180	0.0174	0.0110
			Settling time (sec)	49.77	45.10	36.84
		Area 03	|Peak Mag| (Hz)	0.0177	0.0172	0.0112
			Settling time (sec)	48.48	44.78	36.52
		Area 04	|Peak Mag| (Hz)	0.0199	0.0192	0.0124
			Settling time (sec)	48.06	43.58	35.98

Table 3: ITAE of the proposed controller.

S. No	Case	Area	PID controller	Fuzzy controller	Proposed controller
1.	Case 01	Area 01	0.5023	0.2917	0.2740
		Area 02	0.2318	0.2101	0.1681
		Area 03	2.6951	1.0208	0.8179
		Area 04	0.8214	0.8110	0.7676
2.	Case 02	Area 01	0.4797	0.2778	0.2770
		Area 02	0.1803	0.1595	0.1592
		Area 03	2.1758	0.9932	0.7964
		Area 04	0.8200	0.8051	0.7526
3.	Case 03	Area 01	0.4952	0.2868	0.2859
		Area 02	0.1861	0.1646	0.1644
		Area 03	2.2460	1.0253	0.8220
		Area 04	0.8388	0.8225	0.7729
4.	Case 04	Area 01	0.4970	0.2886	0.2711
		Area 02	0.2294	0.2079	0.1663
		Area 03	2.6667	1.0100	0.8092
		Area 04	0.8127	0.8025	0.7595

zero frequency deviation compared to other controllers, as shown in Figures 20–23.

Table 2 shows the MATLAB/Simulink's numerical results for the prescribed four-area power system network for frequency deviation using different types of controllers and power generation cost using different optimization techniques. In addition to this, the ANFIS controller [48] was also tested for the considered network to mitigate frequency deviation problems. However, the performance was almost the same as that of the fuzzy controller. It was found that the

LFC with LSTM provided the best performance with minimum overshoot and settling time compared to the other two considered controllers in all four areas. As discussed in Section 3, the accuracy of the proposed LSTM RNN methodology can be assessed with the help of ITAE and the corresponding numerical figures for all the 4 considered scenarios that are given in Table 3. It is clear from the results that the ITAE of the proposed methodology was well minimized by about 6.54% to 69.65% compared to other controllers. Power generation cost was also calculated for all the four distinct situations and depicted in Figure 24. It is clear that the application of the hybrid algorithm performs well in optimizing the flexible load demand so that the optimum generation cost can be obtained with the consideration of bounds in system frequency.

6. Conclusion

This work discussed the effect of fast and unpredictable power variations generated by intermittent power generation sources and electric vehicles on the frequency stability of modern power systems. Active power fluctuations in real-time were investigated using a deep learning strategy based on a long short-term memory recurrent neural network. The observed power fluctuations could be used as a control reference for automatic generation control to maintain better system frequency and obtain optimum generation cost with the use of FA/FPA based demand management techniques. The suggested method was applied to the realistic model of an Indian power system integrated with distributed generation technology and validated and compared to the classical methods. Simulation results revealed decent improvements in frequency response performance indices, as the maximum peak overshoot was decreased by 21.25% to 51.2%, settling time was lowered by about 23.34% to 65.40% and ITAE was minimized about 6.54% to 69.65% for the suggested control technique compared to other controllers. The simulation results clearly indicate the importance of power fluctuation identification as well as the benefits of the proposed strategy. The findings show that the proposed technique was successful in improving controller performance by minimizing performance characteristics such as peak overshoot, settling time, and ITAE.

Nomenclature

Abbreviations

ACO: Ant colony optimization
ALO: Ant lion optimizer
ACE: Area control error
AGC: Automatic generation control
BESS: Battery energy storage system
CO: Chimp optimization
DMT: Demand management technique
EV: Electric vehicle
FA: Firefly algorithm
FA/FPA: Firefly algorithm hybridized with flower pollination algorithm
FPA: Flower pollination algorithm
IAE: Integral absolute error
ISE: Integral squared error
ITAE: Integral time absolute error
ITSE: Integral time-weighted-squared error
LFC: Load frequency control
LSTM: Long short-term memory
PSO: Particle swarm optimization
PFC: Primary frequency control
RBFNN: Radial basis function neural network
RNN: Recurrent neural network
SFC: Secondary frequency control

Parameters

ΔF_{UL}: Dead band upper limit
ΔF_{LL}: Dead band lower limit
ΔP_{AG}^{max}: Maximum power output of the EV fleet
ΔP_{AG}^{min}: Minimum power output of the EV fleet
R_{AG}: Model droop coefficient
K_{EV}: EV gain
N_{EV}: Number of connected EVs
T_{EV}: Battery time constant
ΔP_{EV}: Incremental generation change of EV fleet
H: Inertia of the synchronous machine
ΔP_D: Variation in electrical power demand
$\Delta P_{tie,ij}$: Variation in tie line power between the i^{th} and j^{th} area
$\Delta P_{m\,d}$: Variation in the turbine output power
ΔP_w: Variation in wind generator output power
$\Delta P_{\sin\,v}$: Variation in solar inverter output power
D: Machine damping coefficient
Δf_i: Frequency deviation of the i^{th} area
T_T: Turbine time constant
$\Delta P_{g\,d}$: Variation in the governor output
ΔP_s: Variation in solar power
T_g: Governor time constant
B: Frequency bias constant
R: Governor droop constant
T_{inv}: Inverter time constant
U: Input variable vector
Y: Output variable vector
X: State variable vector
W: Disturbance vector
i: Input gate
f: Forget gate
o: Output gate
σ: Sigmoid activation function
W: Weight matrices
$\tilde{C}$: Candidate hidden state
C_t: Internal memory of the unit
h_t: Final output of the memory unit
n: Number of areas
K_p: Proportional controller gain
K_i: Integral controller gain
K_d: Derivative controller gain
$\Delta V_{\min,i}$: Variation in minimum voltage
ΔP_d: Variation in electrical power demand
N_p: Number of conventional thermal units
N_c: Number of cogeneration units
$C_i(P_i^p)$: Fuel cost of the conventional thermal units

$C_j(P_j^c, H_j^c)$ Fuel cost of the cogeneration units
:
P_i^p: Power generation of the i^{th} conventional thermal unit
P_j^c: Power generation of the j^{th} cogeneration thermal unit
$\alpha_i, \beta_i, \gamma_i$: Cost coefficients of the conventional thermal units
a_j, b_j, c_j: Cost coefficients of the cogeneration units.

Data Availability

DATA reffered byReference [47] used.

Conflicts of Interest

The authors declare that there are no conflicts of interest regarding the publication of this paper.

References

[1] M. Khalili, M. Ali Dashtaki, M. A. Nasab, H. Reza Hanif, S. Padmanaban, and B. Khan, "Optimal instantaneous prediction of voltage instability due to transient faults in power networks taking into account the dynamic effect of generators," *Cogent Engineering*, vol. 9, no. 1, Article ID 2072568, 2022.

[2] M. A. Dashtaki, H. Nafisi, A. Khorsandi, M. Hojabri, and E. Pouresmaeil, "Dual two-level voltage source inverter virtual inertia emulation: a comparative study," *Energies*, vol. 14, no. 4, p. 1160, 2021.

[3] S.-J. Zhou, H.-B. Zeng, and H.-Q. Xiao, "Load frequency stability analysis of time-delayed multi-area power systems with EV aggregators based on Bessel-Legendre inequality and model reconstruction technique," *IEEE Access*, vol. 8, pp. 99948–99955, 2020.

[4] K. S. Ko and D. K. Sung, "The effect of EV aggregators with time-varying delays on the stability of a load frequency control system," *IEEE Transactions on Power Systems*, vol. 33, no. 1, pp. 669–680, 2018.

[5] A. Khalil and A. S. Peng, "Delay margin computation for load frequency control system with plug-in electric vehicles," *International Journal of Power and Energy Systems*, vol. 38, no. 3, pp. 1–17, 2018.

[6] A. Naveed, Ş. Sönmez, and S. Ayasun, "Impact of electric vehicle aggregator with communication time delay on stability regions and stability delay margins in load frequency control system," *Journal of Modern Power Systems and Clean Energy*, vol. 9, no. 3, pp. 595–601, 2021.

[7] T. N. Pham, S. Nahavandi, L. V. Hien, H. Trinh, and K. P. Wong, "Static output feedback frequency stabilization of time-delay power systems with coordinated electric vehicles state of charge control," *IEEE Transactions on Power Systems*, vol. 32, no. 5, pp. 3862–3874, 2017.

[8] H. Fan, L. Jiang, and C. Mao, "Frequency regulation of multi-area power systems with plug-in electric vehicles considering communication delays," *IET Generation, Transmission & Distribution*, vol. 10, no. 14, pp. 3481–3491, 2016.

[9] R. Jorge, M. A. Matos, and F. J. Soares, "Framework for the participation of EV aggregators in the electricity market," in *Proceedings of the 2014 IEEE International Electric Vehicle Conference (IEVC)*, Florence, Italy, 2014.

[10] A. M. Carreiro, H. M. Jorge, and C. H. Antunes, "Energy management systems aggregators: a literature survey," *Renewable and Sustainable Energy Reviews*, vol. 73, pp. 1160–1172, 2017.

[11] W. Kempton and J. Tomić, "Vehicle-to-grid power implementation: from stabilizing the grid to supporting large-scale renewable energy," *Journal of Power Sources*, vol. 144, no. 1, pp. 280–294, 2005.

[12] Y. Mu, J. Wu, J. Ekanayake, N. Jenkins, and H. Jia, "Primary frequency response from electric vehicles in the Great Britain power system," *IEEE Transactions on Smart Grid*, vol. 4, no. 2, pp. 1142–1150, 2013.

[13] W. Hu, C. Su, Z. Chen, and B. Bak-Jensen, "Optimal operation of plug-in electric vehicles in power systems with high wind power penetrations," *IEEE Transactions on Sustainable Energy*, vol. 4, no. 3, pp. 577–585, 2013.

[14] I. Ngamroo, "V 2 G-based PHEV for load-frequency control and its capacity reduction effect on BESS in A smart grid with wind power penetration," *International Review on Modelling and Simulations*, vol. 5, p. 3, 2012.

[15] H. Liu, Z. Hu, Y. Song, and J. Lin, "Decentralized vehicle-to-grid control for primary frequency regulation considering charging demands," *IEEE Transactions on Power Systems*, vol. 28, no. 3, pp. 3480–3489, 2013.

[16] S. Vachirasricirikul and I. Ngamroo, "Robust LFC in a smart grid with wind power penetration by coordinated V2G control and frequency controller," *IEEE Transactions on Smart Grid*, vol. 5, no. 1, pp. 371–380, 2014.

[17] J. Pahasa and I. Ngamroo, "PHEVs bidirectional charging/discharging and SoC control for microgrid frequency stabilization using multiple MPC," *IEEE Transactions on Smart Grid*, vol. 6, no. 2, pp. 526–533, 2015.

[18] H. Yang, C. Y. Chung, and J. Zhao, "Application of plug-in electric vehicles to frequency regulation based on distributed signal acquisition via limited communication," *IEEE Transactions on Power Systems*, vol. 28, no. 2, pp. 1017–1026, 2013.

[19] S. Izadkhast, P. Garcia-Gonzalez, and P. Frías, "An aggregate model of plug-in electric vehicles for primary frequency control," *IEEE Transactions on Power Systems*, vol. 30, no. 3, pp. 1475–1482, 2015.

[20] J. R. Pillai and B. Bak-Jensen, "Integration of vehicle-to-grid in the western Danish power system," *IEEE Transactions on Sustainable Energy*, vol. 2, no. 1, pp. 12–19, 2010.

[21] H. Liu, Z. Hu, Y. Song, J. Wang, and Xu Xie, "Vehicle-to-grid control for supplementary frequency regulation considering charging demands," *IEEE Transactions on Power Systems*, vol. 30, no. 6, pp. 3110–3119, 2015.

[22] M. Takagi, K. Yamaji, and H. Yamamoto, "Power system stabilization by charging power management of plug-in hybrid electric vehicles with LFC signal," in *Proceedings of the 2009 IEEE Vehicle Power and Propulsion Conference*, Dearborn, MI, USA, 2009.

[23] T. Masuta and A. Yokoyama, "Supplementary load frequency control by use of a number of both electric vehicles and heat pump water heaters," *IEEE Transactions on Smart Grid*, vol. 3, no. 3, pp. 1253–1262, 2012.

[24] M. D. Galus, S. Koch, and G. Andersson, "Provision of load frequency control by PHEVs, controllable loads, and a cogeneration unit," *IEEE Transactions on Industrial Electronics*, vol. 58, no. 10, pp. 4568–4582, 2011.

[25] I. Ngamroo, "Specified structure mixed h2/h8 control-based robust frequency stabilization in a smart grid by plug-in hybrid electric vehicles," *International Journal of Innovative*

Computing, Information and Control, vol. 9, no. 1, pp. 81–97, 2013.

[26] M. Datta and T. Senjyu, "Fuzzy control of distributed PV inverters/energy storage systems/electric vehicles for frequency regulation in a large power system," *IEEE Transactions on Smart Grid*, vol. 4, no. 1, pp. 479–488, 2013.

[27] P. M. R. Almeida, F. Soares, and J. A. P. Lopes, "Electric vehicles contribution for frequency control with inertial emulation," *Electric Power Systems Research*, vol. 127, pp. 141–150, 2015.

[28] S. Vachirasricirikul and I. Ngamroo, "Robust controller design of heat pump and plug-in hybrid electric vehicle for frequency control in a smart microgrid based on specified-structure mixed H2/H∞ control technique," *Applied Energy*, vol. 88, no. 11, pp. 3860–3868, 2011.

[29] K. Ranjitha, P. Sivakumar, M. Monica, and R. Elavarasu, "Swarm intelligence based load frequency control of two area thermal system–comparative analysis," in *Proceedings of the 2020 4th International Conference on Electronics, Communication and Aerospace Technology (ICECA)*, Coimbatore, India, 2020.

[30] K. Ranjitha, P. Sivakumar, R. Elavarasu, and M. Monica, "Load frequency controller based on ant colony and firefly algorithm optimization-A review AIP Conference Proceedings," *AIP Publishing LLC*, vol. 2405, no. 1, Article ID 040020, 2022.

[31] G. Soorya Priya and P. Sivakumar, "Analysis of antlion optimizer-based ABT for automatic generation control of an interconnected power system," *Soft Computing*, vol. 23, no. 18, pp. 8563–8577, 2019.

[32] J. Kennedy, "Particle swarm optimization," *Encyclopedia of machine learning*, vol. 760, p. 766, 2011.

[33] K. Ranjitha, P. Sivakumar, R. Elavarasu, M. Monica, and A. Rajapandiyan, "Firefly algorithm optimized load frequency controller for multi-source power system," in *Proceedings of the 2021 Emerging Trends in Industry 4.0 (ETI 4.0)*, Raigarh, India, 2021.

[34] K. Ranjitha, P. Sivakumar, and M. Monica, "Load frequency control based on an improved Chimp optimization algorithm using adaptive weight strategy," *COMPEL-the International Journal for Computation and Mathematics in Electrical and Electronic Engineering*, vol. 41, no. 5, pp. 1618–164, 2022.

[35] K. Liao and Y. Xu, "A robust load frequency control scheme for power systems based on second-order sliding mode and extended disturbance observer," *IEEE Transactions on Industrial Informatics*, vol. 14, no. 7, pp. 3076–3086, 2018.

[36] C. Wang, Y. Mi, Y. Fu, and P. Wang, "Frequency control of an isolated micro-grid using double sliding mode controllers and disturbance observer," *IEEE Transactions on Smart Grid*, vol. 9, no. 2, pp. 923–930, 2018.

[37] G. Lou, W. Gu, J. Wang, J. Wang, and B. Gu, "A unified control scheme based on a disturbance observer for seamless transition operation of inverter-interfaced distributed generation," *IEEE Transactions on Smart Grid*, vol. 9, no. 5, pp. 5444–5454, 2018.

[38] H. Yang, Y. Zhang, J. Liang, J. Liu, N. Zhang, and P. D. Walker, "Robust deadbeat predictive power control with a discrete-time disturbance observer for PWM rectifiers under unbalanced grid conditions," *IEEE Transactions on Power Electronics*, vol. 34, no. 1, pp. 287–300, 2019.

[39] G. Pannocchia and A. Bemporad, "Combined design of disturbance model and observer for offset-free model predictive control," *IEEE Transactions on Automatic Control*, vol. 52, no. 6, pp. 1048–1053, 2007.

[40] W. Kong, Z. Y. Dong, Y. Jia, D. J. Hill, Y. Xu, and Y. Zhang, "Short-term residential load forecasting based on LSTM recurrent neural network," *IEEE Transactions on Smart Grid*, vol. 10, no. 1, pp. 841–851, 2019.

[41] Z. Yun, Q. Zhou, C. Sun, S. Lei, Y. Liu, and S. Yang, "RBF neural network and ANFIS-based short-term load forecasting approach in real-time price environment," *IEEE Transactions on Power Systems*, vol. 23, no. 3, pp. 853–858, 2008.

[42] Yu Ma and Y. Cai, "A fuzzy model predictive control based upon adaptive neural network disturbance observer for a constrained hypersonic vehicle," *IEEE Access*, vol. 6, pp. 5927–5938, 2018.

[43] Yu Kurita, Y. Moriya, and S. Iwamoto, "Control of storage batteries using a disturbance observer in load frequency control for large wind power penetration," in *Proceedings of the 2015 IEEE Power & Energy Society General Meeting*, Denver, CO, USA, 2015.

[44] K. Greff, R. K. Srivastava, J. Koutnik, B. R. Steunebrink, and J. Schmidhuber, "LSTM: a search space odyssey," *IEEE Transactions on Neural Networks and Learning Systems*, vol. 28, no. 10, pp. 2222–2232, 2017.

[45] M. Zand, M. A. Nasab, P. Sanjeevikumar, P. K. Maroti, and J. B. Holm-Nielsen, "Energy management strategy for solid-state transformer-based solar charging station for electric vehicles in smart grids," *IET Renewable Power Generation*, vol. 14, pp. 3843–3852, 2020.

[46] M. Zand, M. A. Nasab, M. Khoobani, A. Jahangiri, S. H. Hosseinian, and A. H. Kimiai, "Robust speed control for induction motor drives using STSM control," in *Proceedings of the 2021 12th Power Electronics, Drive Systems, and Technologies Conference (PEDSTC)*, Tabriz, Iran, 2021.

[47] K. Ranjitha, S. Ponnurangam, and A. Rajapandiyan, "Impact of demand management with load frequency control in distribution network with high penetration of renewable energy sources," *International Transactions on Electrical Energy Systems*, vol. 31, p. 11, 2021.

[48] L. Tightiz, M. A. Nasab, H. Yang, and A. Addeh, "An intelligent system based on optimized ANFIS and association rules for power transformer fault diagnosis," *ISA Transactions*, vol. 103, pp. 63–74, 2020.